

Bim suppresses the development of SLE by limiting myeloid inflammatory responses

FuNien Tsai,¹ Philip J. Homan,¹ Hemant Agrawal,³ Alexander V. Misharin,² Hiam Abdala-Valencia,¹ G. Kenneth Haines III,⁴ Salina Dominguez,¹ Christina L. Bloomfield,¹ Rana Saber,¹ Anthony Chang,⁵ Chandra Mohan,⁶ Jack Hutcheson,⁷ Anne Davidson,⁸ G.R. Scott Budinger,² Philippe Bouillet,⁹ Andrea Dorfleutner,¹ Christian Stehlik,¹ Deborah R. Winter,¹ Carla M. Cuda,¹ and Harris Perlman¹

¹Division of Rheumatology, Feinberg School of Medicine and ²Division of Pulmonary and Critical Care, Feinberg School of Medicine, Northwestern University, Chicago, IL

³TTP Labtech India Private Limited, Faridabad, India

⁴Department of Pathology, Icahn School of Medicine at Mount Sinai, New York, NY

⁵Department of Pathology, University of Chicago, Chicago, IL

⁶Department of Biomedical Engineering, University of Houston, Houston, TX

⁷Tri-Service Research Laboratory, San Antonio, TX

⁸The Feinstein Institute for Medical Research, Hofstra Northwell School of Medicine, Manhasset, NY

⁹The Walter and Eliza Hall Institute of Medical Research, Parkville, Victoria, Australia

The Bcl-2 family is considered the guardian of the mitochondrial apoptotic pathway. We demonstrate that Bim acts as a molecular rheostat by controlling macrophage function not only in lymphoid organs but also in end organs, thereby preventing the break in tolerance. Mice lacking Bim in myeloid cells ($LysM^{Cre}Bim^{fl/fl}$) develop a systemic lupus erythematosus (SLE)-like disease that mirrors aged $Bim^{-/-}$ mice, including loss of marginal zone macrophages, splenomegaly, lymphadenopathy, autoantibodies (including anti-DNA IgG), and a type I interferon signature. $LysM^{Cre}Bim^{fl/fl}$ mice exhibit increased mortality attributed to glomerulonephritis (GN). Moreover, the toll-like receptor signaling adaptor protein TRIF (TIR-domain-containing adapter-inducing interferon- β) is essential for GN, but not systemic autoimmunity in $LysM^{Cre}Bim^{fl/fl}$ mice. Bim-deleted kidney macrophages exhibit a novel transcriptional lupus signature that is conserved within the gene expression profiles from whole kidney biopsies of patients with SLE. Collectively, these data suggest that the Bim may be a novel therapeutic target in the treatment of SLE.

INTRODUCTION

Systemic lupus erythematosus (SLE) is a multifactorial, multigenetic autoimmune disease of unknown etiology that is characterized by the presence of autoantibodies and severe end-organ damage (Shirai and Hirose, 2006). The origin of the break in tolerance leading to the development of systemic autoimmunity and production of autoantibodies is unknown. However, studies have suggested that a failure to process apoptotic body antigens by marginal zone macrophages (MZMs) may be required for the activation of lymphocytes in SLE-like disease (McGaha and Karlsson, 2016).

Monocytes and macrophages are mononuclear phagocytes that are crucial for maintaining homeostasis (Ginhoux and Jung, 2014). Macrophages are highly plastic and are there-

fore credited with essential roles in inflammation as well as tissue injury and repair (Ginhoux and Jung, 2014). Recent studies have shown that, similar to peripheral blood monocytes, renal macrophages from SLE patients are increased in number and exhibit elevated expression of activation markers (Katsiari et al., 2010). Further, the numbers of glomerular macrophages, tubular luminal macrophages and/or CD16⁺ macrophages in the kidney correlate with clinical activity and outcome in patients with SLE (Hill et al., 2001). Studies in murine models also support the importance of monocytes and macrophages in the pathogenesis of SLE-like disease (Hutcheson et al., 2008; Katsiari et al., 2010). Collectively, these data suggest a pivotal role for monocytes and macrophages in the pathogenesis of SLE and SLE-like disease, but the factors that control their state of activation and function are unknown.

Apoptosis or programmed cell death is necessary for immune cell development and homeostasis. Cells undergo apoptosis through two distinct pathways: an extrinsic path-

Correspondence to Carla M. Cuda: c-cuda@northwestern.edu; Harris Perlman: h-perlman@northwestern.edu

Abbreviations used: ANA, antinuclear autoantibody; BH, Bcl-2 homology; BMDM, bone marrow-derived macrophage; CTRL, control; DC, dendritic cell; dsDNA, double-stranded DNA; EdU, 5-ethynyl-2'-deoxyuridine; FDR, false discovery rate; GN, glomerulonephritis; LN, lupus nephritis; MMM, marginal metallophilic macrophage; MZB, marginal zone B; MZM, marginal zone macrophage; PAS, periodic acid-Schiff base; pDC, plasmacytoid DC; RNA-seq, RNA sequencing; RPM, red pulp macrophage; SLE, systemic lupus erythematosus; SNP, single-nucleotide polymorphism; ssDNA, single-stranded DNA; TRIF, TIR-domain-containing adapter-inducing interferon- β .

© 2017 Tsai et al. This article is distributed under the terms of an Attribution-Noncommercial-Share Alike-No Mirror Sites license for the first six months after the publication date (see <http://www.rupress.org/terms/>). After six months it is available under a Creative Commons License (Attribution-Noncommercial-Share Alike 4.0 International license, as described at <https://creativecommons.org/licenses/by-nc-sa/4.0/>).



way of apoptosis and an intrinsic pathway of apoptosis. Specifically, the intrinsic pathway is regulated by the Bcl-2 (B cell lymphoma 2) protein family and proceeds through a mitochondrial-dependent mechanism. Antiapoptotic proteins of the Bcl-2 protein family include Bcl-2, Bcl-xL, Bcl-w, Mcl-1, and A1. Proapoptotic proteins of the Bcl-2 protein family consist of two types: those with multiple Bcl-2 homology (BH) domains, including Bak, Bax, Bok, and Bcl-x5 and those containing only a single BH3 domain, including Bim, Bad, Bid, Noxa, and Puma. Studies using BH3 peptides reveal that Bid, Bim, and Puma may function as direct activators of apoptosis, whereas Bad and Noxa exist as indirect activators of cell death (Billard, 2013). However, only mice deficient in Bim develop spontaneous systemic autoimmunity (Bouillet et al., 1999). Given the role of Bim as a mediator of cell death and the lymphocyte-centric hypothesis of SLE development, significant attention has understandably been paid to the role that Bim plays in eliminating self-reactive lymphocytes. However, Bim deficiency also impacts innate immune cell populations (Hutcheson et al., 2008). Little is known about the role of Bim on innate immune cells or their relative contribution to systemic autoimmunity. In this study, we demonstrate that myeloid cells are central initiators of SLE-like disease in Bim^{-/-} mice and potentially dispute the conventional dogma that the central role of Bim in autoimmune disease is to prevent the escape of autoreactive lymphocytes from apoptosis. Novel strategies that target Bim may be useful for the treatment of systemic autoimmunity.

RESULTS

Mice deficient for Bim in macrophages develop SLE-like disease

We and others have reported that Bim^{-/-} mice develop systemic autoimmunity and end-stage glomerulonephritis (GN; Bouillet et al., 1999; Hutcheson et al., 2008). To determine whether Bim might prevent systemic autoimmunity via its function in myeloid cells, we generated mice with conditional deletion of Bim in the myeloid cell compartment on a mixed background (LysM^{Cre}Bim^{fl/fl}) and compared them to age- and sex-matched control mice (LysM^{+/+}Bim^{fl/fl}, LysM^{Cre}Bim^{+/+}, CD19^{Cre}Bim^{fl/fl}, and CD4^{Cre}Bim^{fl/fl}). At 6 mo of age, female LysM^{Cre}Bim^{fl/fl} mice showed disrupted splenic architecture (Fig. 1 A) and developed severe GN (Fig. 1, B–D). LysM^{Cre}Bim^{fl/fl} mice also showed higher kidney scores than control mice (Fig. 1 C). In contrast, mice deficient for Bim in B or T cells did not exhibit any features of systemic autoimmunity, GN (Fig. 1, A–D), or enhanced mortality (Fig. 1 E).

Mice on a 129 background have a predisposition to lupus disease (Obata et al., 1979); therefore, we backcrossed LysM^{Cre}Bim^{fl/fl} mice onto a C57BL/6 background. Genomic screening of 150 single-nucleotide polymorphism (SNP) markers confirmed that LysM^{Cre}Bim^{fl/fl} mice are 98% on the C57BL/6 genetic background (Fig. S1 A and Table S1). 8-mo-old female LysM^{Cre}Bim^{fl/fl} mice exhibited severe splenomegaly and lymphadenopathy compared with con-

trols (Fig. 2, A–E). Enlargement of the spleen was associated with abnormal splenic architecture marked by distention of red pulp area and lymphoid hyperplasia in white pulp area (Fig. 2 C). There was a substantial increase in antinuclear autoantibody (ANA) titers in LysM^{Cre}Bim^{fl/fl} mice (Fig. 2 F), including anti-single-stranded DNA (anti-ssDNA) and anti-double-stranded DNA (anti-dsDNA) IgG ANA. LysM^{Cre}Bim^{fl/fl} mice also showed increased IgM ANA directed against ssDNA, dsDNA, histones, and nucleosomes (Fig. 2 F). Additionally, Ig isotypes, in particular the pathogenic IgG2a and IgG2b subclasses, were elevated in LysM^{Cre}Bim^{fl/fl} mice (Fig. 2 G). Moreover, the serum levels of IL-12p70, IL-17, IFN-β, and IFN-γ were higher in LysM^{Cre}Bim^{fl/fl} mice (Fig. 2, H–J). LysM^{Cre}Bim^{fl/fl} mice also had evidence of IgG- and IgM-immune complex deposition in kidneys (Fig. 2 K), increased proteinuria (Fig. 2 L), and severe GN (Fig. 2, M and N). Further, deleting Bim did not affect the balance of the Bcl-2 family members in splenic macrophages (Fig. S1, B and C). Although the expression levels of *Bcl-2* and *Bcl-xL* were lower in 3- and 8-mo-old LysM^{Cre}Bim^{fl/fl} kidney macrophages, the other Bcl-2 family members, including *Bcl-w*, *Mcl-1*, *Bax*, and *Bak*, were unaffected (Fig. S1, D and E).

LysM^{Cre}Bim^{fl/fl} mice showed altered splenic cellularity

We next examined the topographical localization of macrophages in spleen of LysM^{Cre}Bim^{fl/fl} mice. It has been well established that Siglec-1 (CD169; Sialoadhesin) and DC-SIGN (CD209b) delineate marginal metallophilic macrophages (MMMs) and MZMs, respectively (McGaha and Karlsson, 2016). MZMs were markedly reduced in LysM^{Cre}Bim^{fl/fl} mice as early as 3 mo of age, and this loss dramatically progressed with age (Fig. 3 A). In contrast, MMM topography were maintained in the spleens of young LysM^{Cre}Bim^{fl/fl} mice, although there was a slight decrease as LysM^{Cre}Bim^{fl/fl} aged (Fig. 3 A). We then used multiparameter flow cytometry to quantify the numbers of MZMs and MMMs in spleen. MZMs and MMMs were gated via the exclusion of doublets, dead cells, red-pulp macrophages (RPMs), lineage⁺ and CD19⁺/B220⁺ cells, and CD209b⁺ and CD169⁺ cells, respectively (Fig. S2, A and B). The expression of CD11b further divided MZMs and MMMs into two subtypes: the CD11b⁺ and CD11b⁻ populations. MZMs were larger in size as measured by diameter (CD11b⁺ MZMs: 29.03 ± 1.58 μm; CD11b⁻ MZMs: 25.87 ± 1.48 μm) than MMMs (CD11b⁺ MMMs: 25.00 ± 1.22 μm; CD11b⁻ MMMs: 21.61 ± 0.42 μm; Fig. S2, C and D; CD11b^{+/+} MZMs vs. CD11b^{+/-} MMMs, P < 0.05). The number of CD11b⁺ MZMs was significantly lower in LysM^{Cre}Bim^{fl/fl} spleens than in control mice at 3 mo of age (Fig. 3 B). The number of CD11b⁺ MZMs and CD11b⁻ MZMs further decreased in LysM^{Cre}Bim^{fl/fl} spleens at 8 mo (Fig. 3, B and C). In contrast, there was no significant difference in the number of CD11b⁺ MMMs between control and LysM^{Cre}Bim^{fl/fl} mice (Fig. 3 D). However, CD11b⁻ MMM numbers increased in 8-mo-old LysM^{Cre}Bim^{fl/fl} mice (Fig. 3 E). LysM^{Cre}Bim^{fl/fl} MZMs and MMMs also displayed enhanced costimulatory signals, including CD80 and CD86 as compared

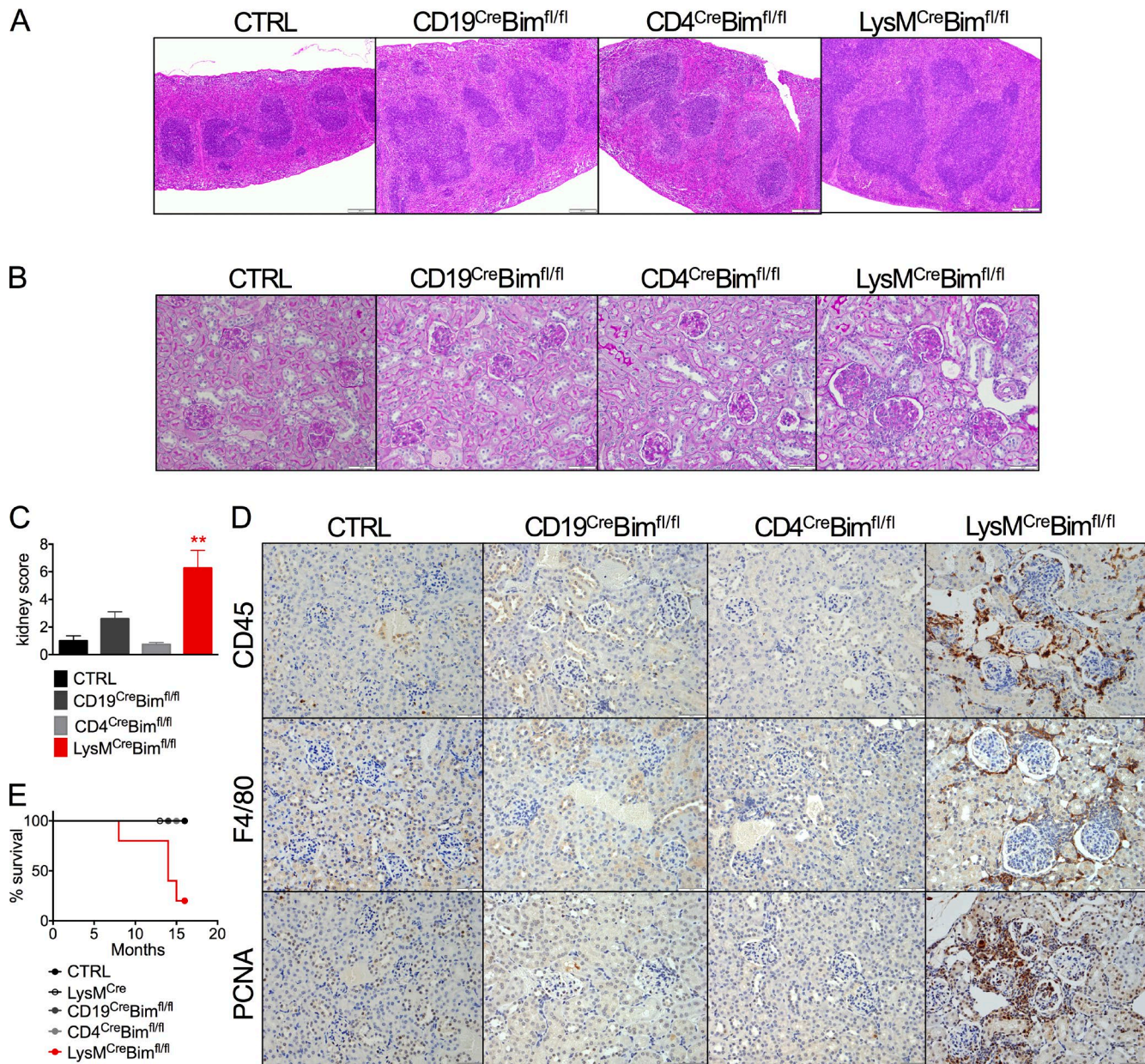


Figure 1. Mice deficient for Bim in monocytes/macrophages on a mixed background display SLE-like disease. 6-mo-old female CTRL ($n \geq 5$), LysM^{Cre} ($n \geq 4$), CD19^{Cre}Bim^{fl/fl} (C57BL/6:129, $n \geq 3$), CD4^{Cre}Bim^{fl/fl} (C57BL/6:129, $n \geq 2$), and LysM^{Cre}Bim^{fl/fl} (C57BL/6:129, $n \geq 5$) mice were examined for systemic autoimmune disease. (A) Abnormality of splenic architecture in LysM^{Cre}Bim^{fl/fl} mice. Representative photomicrographs of H&E-stained spleen sections. Bars, 200 μ m. (B) Representative photomicrographs of PAS-stained kidney sections. Bars, 50 μ m. (C) Kidney sections scored for kidney damage by a pathologist blinded to the study. (D) Representative photomicrographs of kidney sections stained with anti-CD45, anti-F4/80, and anti-PCNA antibodies. Bars, 50 μ m. (E) Survival curve. Data were obtained from the indicated number of mice in three individual experiments. Data are presented as mean \pm SEM and were compared by Mann-Whitney test. Asterisks indicate a significant difference between Cre (e.g., LysM^{Cre}Bim^{fl/fl}) and CTRL (**, $P < 0.01$).

with controls (Fig. S2, E–H). Because marginal zone B (MZB) cells maintain close contact with MZMs under steady-state condition, we observed a thinner layer of CD1d⁺ MZB cells in the splenic MZ region of LysM^{Cre}Bim^{fl/fl} mice (Fig. S2, I and J). We then performed RNA sequencing (RNA-seq) on the CD11b⁺ and CD11b⁻ populations of MZMs in order to assess

transcriptional changes caused by Bim deletion. The presence or absence of CD11b elicited more variation in gene expression than the deletion of Bim (Fig. 3 F). CD11b⁺ MZMs and CD11b⁻ MZMs exhibited 20 and 64 differentially expressed genes, respectively, when Bim was deleted, including *Lyz2*, *Hjurf*, and *Ms4a6d* (Fig. 3, G and H).

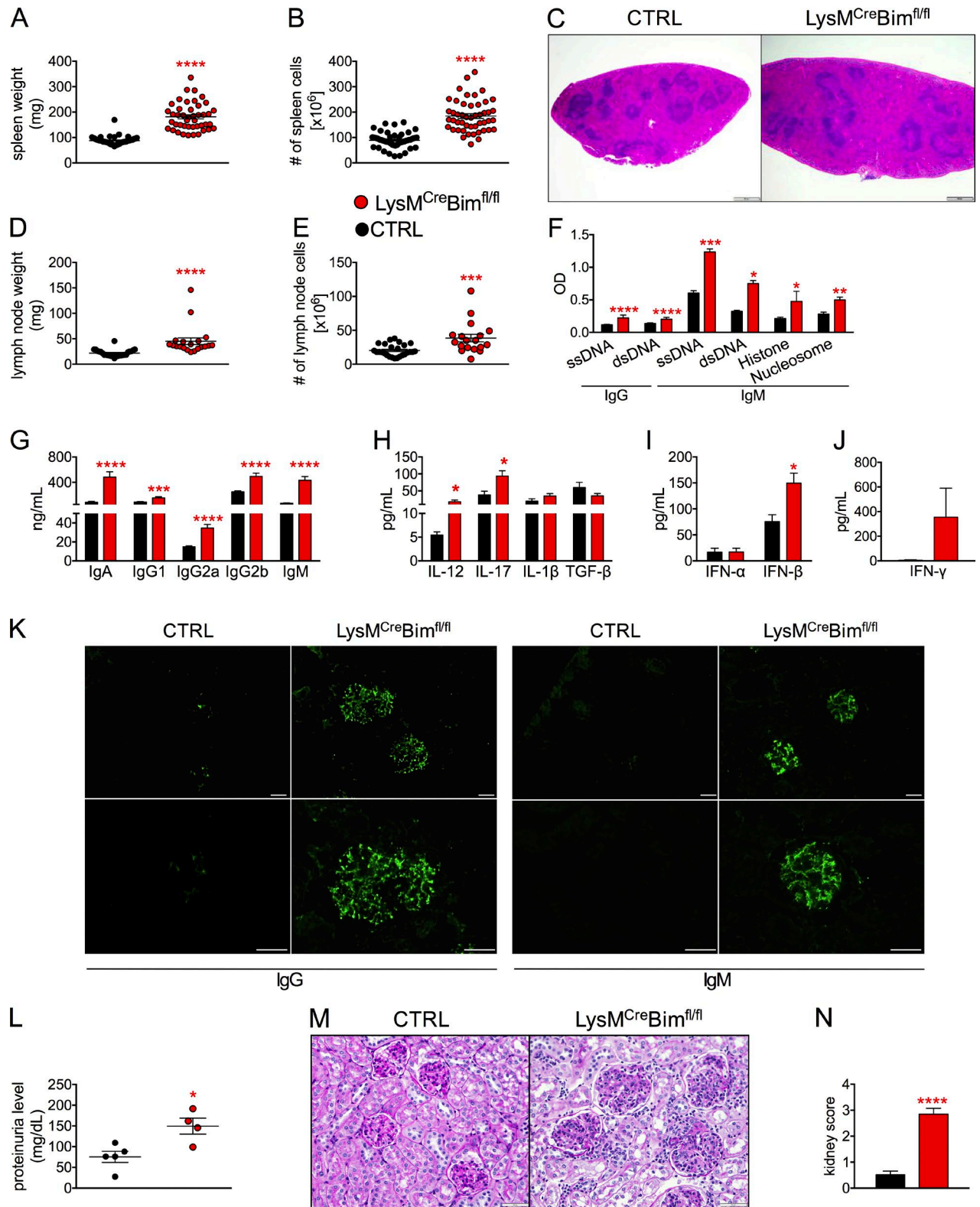


Figure 2. **Loss of Bim in myeloid cells, including macrophages, leads to a break in tolerance and the development of SLE-like disease.** 8-mo-old female CTRL and *LysM^{Cre}Bim^{fl/fl}* (C57BL/6) mice were examined for systemic autoimmune disease phenotypes. (A) Spleen weights for CTRL ($n = 51$) and *LysM^{Cre}Bim^{fl/fl}* ($n = 44$) mice. (B) Total number of live spleen cells from CTRL ($n = 24$) and *LysM^{Cre}Bim^{fl/fl}* ($n = 19$) mice. (C) Representative photomicrographs of H&E-stained spleen sections. Bars, 200 μ m. (D) Cervical and inguinal lymph node weights for CTRL ($n = 26$) and *LysM^{Cre}Bim^{fl/fl}* ($n = 20$) mice. (E) Total

We further expanded our studies to examine the splenic cellular composition of $\text{LysM}^{\text{Cre}}\text{Bim}^{\text{fl/fl}}$ mice using the flow gating strategy shown in Fig. 4 A. The numbers of monocytes, RPMs (Fig. 4, B–D), plasmacytoid dendritic cells (pDCs; Fig. 4 E) and CD11b^- dendritic cells (DCs; Fig. 4 F) were elevated in $\text{LysM}^{\text{Cre}}\text{Bim}^{\text{fl/fl}}$ mice. Further, both CD4 and CD8 naive, memory, and effector T cells (Fig. 4, G and H) and FoxP3^+ regulatory T cells (Fig. 4 I) showed higher numbers in $\text{LysM}^{\text{Cre}}\text{Bim}^{\text{fl/fl}}$ mice than controls. All B cell types with the exception of MZ and T2 B cells were also greater in number (Fig. 4 J) in $\text{LysM}^{\text{Cre}}\text{Bim}^{\text{fl/fl}}$ mice. The enlargement of the lymphocyte compartment was associated with increased activation of monocytes, RPMs, and DCs, as indicated by elevated levels of CD80, MHCII, and CD40 (Fig. 4, K–R). Furthermore, T cells were hyperactivated, as indicated by the significant increase in CD69 and CD279 expression (Fig. 4, S–Y). T cell proliferation was significantly higher in macrophages and DCs isolated from $\text{LysM}^{\text{Cre}}\text{Bim}^{\text{fl/fl}}$ mice than in those isolated from controls in a mixed leukocyte reaction assay (Fig. 4 Z).

Bim-deleted myeloid cells are sufficient to cause systemic autoimmunity

Previous studies have suggested that the LysM^{Cre} (lysozyme M) transgenic mouse may be promiscuous with respect to its promoter (Miyamoto et al., 2002; Ye et al., 2003). We also observed that hematopoietic cells from $\text{LysM}^{\text{Cre}}\text{Bim}^{\text{fl/fl}}$ mice displayed variable reduction of Bim (Fig. 5 A). Therefore, we adoptively transferred WT CD45.1 lymphocytes into congenic $\text{Rag}^{-/-}\text{LysM}^{\text{Cre}}\text{Bim}^{\text{fl/fl}}$ or $\text{Rag}^{-/-}$ mice once a month for 8 mo (Fig. 5 B). Only $\text{Rag}^{-/-}\text{LysM}^{\text{Cre}}\text{Bim}^{\text{fl/fl}}$ mice that received WT lymphocytes developed splenomegaly (Fig. 5, C and D) and increased lymph node weights (not depicted). The numbers of CD11b^+ MZMs and CD11b^- MZMs were reduced in the spleens of $\text{Rag}^{-/-}\text{LysM}^{\text{Cre}}\text{Bim}^{\text{fl/fl}}$ mice that underwent adoptive transfer (Fig. 5, E and F). In contrast, the numbers of MMMs were mildly affected by the loss of Bim in the $\text{Rag}^{-/-}$ mice (Fig. 5, E and F). Moreover, the significantly expanded lymphocyte pool (Fig. 5 G) was associated with increased activation of monocytes, RPMs and DCs in $\text{Rag}^{-/-}\text{LysM}^{\text{Cre}}\text{Bim}^{\text{fl/fl}}$ mice that underwent adoptive transfer as compared with controls (Fig. S3, A–H). This enhanced activation status was also consistent with $\text{LysM}^{\text{Cre}}\text{Bim}^{\text{fl/fl}}$ mice (Fig. 4, K–R). Serum levels of histone-reactive IgG ANA and ssDNA-reactive IgM ANA after adoptive transfer were significantly elevated in $\text{Rag}^{-/-}\text{LysM}^{\text{Cre}}\text{Bim}^{\text{fl/fl}}$

mice than in $\text{Rag}^{-/-}$ mice (Fig. 5 H). Importantly, in the adoptive transfer group, $\text{Rag}^{-/-}\text{LysM}^{\text{Cre}}\text{Bim}^{\text{fl/fl}}$ mice developed GN, as indicated by higher pathology scores (Fig. 5 I), distorted kidney structure (Fig. 5 J), and increased infiltrating CD45^+ cells and F4/80^+ macrophages in the glomeruli as compared with $\text{Rag}^{-/-}$ mice (Fig. 5 K). Moreover, analysis of Bim expression in $\text{Rag}^{-/-}\text{LysM}^{\text{Cre}}\text{Bim}^{\text{fl/fl}}$ mice after adoptive transfer revealed that the transferred lymphocytes had intact Bim expression, whereas the myeloid cells had consistent loss of Bim (Fig. 5 L). Further, $\text{CD4}^{\text{Cre}}\text{Bim}^{\text{fl/fl}}$ and $\text{dLck}^{\text{Cre}}\text{Bim}^{\text{fl/fl}}$ mice on a C57BL/6 background (Herold et al., 2014; Li et al., 2017) did not display splenomegaly (Fig. S3, I and J) or MZM loss (Fig. S3, K–N). $\text{CD4}^{\text{Cre}}\text{Bim}^{\text{fl/fl}}$ and $\text{dLck}^{\text{Cre}}\text{Bim}^{\text{fl/fl}}$ mice did not develop GN (Fig. S3 O) and showed no significant difference in the numbers of kidney monocytes/macrophages compared with controls (Fig. S3, P and Q). These data demonstrate that the deficiency of Bim in myeloid cells is sufficient to drive the SLE pathology in $\text{LysM}^{\text{Cre}}\text{Bim}^{\text{fl/fl}}$ mice. To further support a potential cell intrinsic effect of Bim deficiency in myeloid cells, we generated mixed bone marrow chimeras by injecting LSK ($\text{Lin}^- \text{Sca1}^+ \text{c-kit}^+$) cells from B6.CD45.1 (CTRL) or/and $\text{LysM}^{\text{Cre}}\text{Bim}^{\text{fl/fl}}$ (CD45.1) donor mice into host $\text{B6.CD45.1}/2$ mice (Fig. 5 M). These chimeric mice developed a mild systemic autoimmune disease at a ratio of 1:1 CTRL and $\text{LysM}^{\text{Cre}}\text{Bim}^{\text{fl/fl}}$ LSK cells (Fig. 5, N–Q).

Bim mediates systemic autoimmunity through its BH3 domain

Because the central function of Bim involves the apoptotic pathway, we examined the effect of Bim deletion on the lifespan of myeloid cells in $\text{LysM}^{\text{Cre}}\text{Bim}^{\text{fl/fl}}$ mice by monitoring EdU (5-ethynyl-2'-deoxyuridine) incorporation and loss over time (Fig. 6 A). Monocytes and neutrophils from various tissues (bone marrow, blood, spleen, and kidney) shared a similar pattern of EdU incorporation at days 35 and 49 (Fig. 6, B–E). Moreover, there was no difference in the loss of EdU between control and $\text{LysM}^{\text{Cre}}\text{Bim}^{\text{fl/fl}}$ monocytes and neutrophils at day 63 (Fig. 6, B–E). pDCs and B cells from the spleen of $\text{LysM}^{\text{Cre}}\text{Bim}^{\text{fl/fl}}$ mice exhibited a lower retention of EdU, whereas little to no difference was observed in control and $\text{LysM}^{\text{Cre}}\text{Bim}^{\text{fl/fl}}$ DCs (Fig. 6 D). EdU-labeling kinetics of macrophages were different in spleen and kidney (Fig. 6, D and E). At day 63, a substantial percentage of $\text{LysM}^{\text{Cre}}\text{Bim}^{\text{fl/fl}}$ RPMs were persistently labeled with EdU (Fig. 6 D), whereas at the same time, $\text{LysM}^{\text{Cre}}\text{Bim}^{\text{fl/fl}}$ kidney macrophages lost EdU labeling

number of live cervical and inguinal lymph node cells from CTRL ($n = 26$) and $\text{Cre}^{\text{LysM}}\text{Bim}^{\text{fl/fl}}$ ($n = 18$) mice. (F–J) Serum from CTRL and $\text{Cre}^{\text{LysM}}\text{Bim}^{\text{fl/fl}}$ mice was measured for levels of IgG and IgM ANA (F and G; CTRL, $n = 27$; $\text{LysM}^{\text{Cre}}\text{Bim}^{\text{fl/fl}}$, $n = 17$); total IgA, IgG, and IgM isotypes (G; CTRL, $n = 22$; $\text{LysM}^{\text{Cre}}\text{Bim}^{\text{fl/fl}}$, $n = 14$), cytokines (H; CTRL, $n = 5$; $\text{LysM}^{\text{Cre}}\text{Bim}^{\text{fl/fl}}$, $n = 7$) and IFN (I and J; CTRL, $n \geq 2$; $\text{LysM}^{\text{Cre}}\text{Bim}^{\text{fl/fl}}$, $n \geq 2$) by ELISA or Luminex assays. (K) Immune complex deposition. Representative photomicrographs of frozen kidney sections stained with FITC-conjugated anti-IgG or anti-IgM antibody. Bars, 50 μm . (L) Proteinuria of CTRL ($n = 5$) and $\text{LysM}^{\text{Cre}}\text{Bim}^{\text{fl/fl}}$ ($n = 5$) mice. (M) Representative photomicrographs of PAS-stained kidney sections. Bars, 50 μm . (N) Kidney sections scored for kidney damage. Data were obtained from the indicated number of mice in three individual experiments. Data are presented as mean \pm SEM and were compared by Mann-Whitney test. Asterisks indicate a significant difference between $\text{LysM}^{\text{Cre}}\text{Bim}^{\text{fl/fl}}$ and CTRL (*, $P < 0.05$; **, $P < 0.01$; ***, $P < 0.001$; ****, $P < 0.0001$).

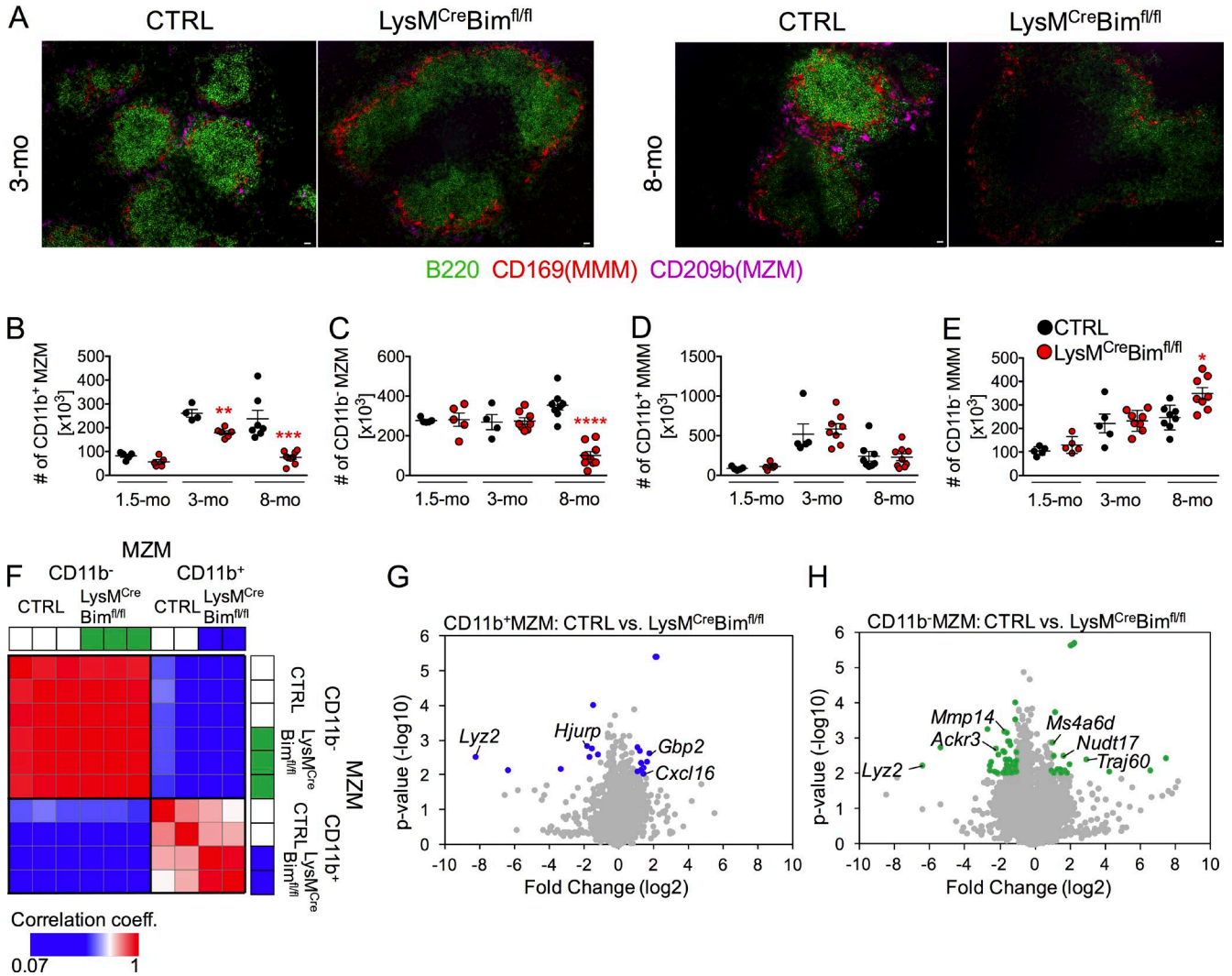
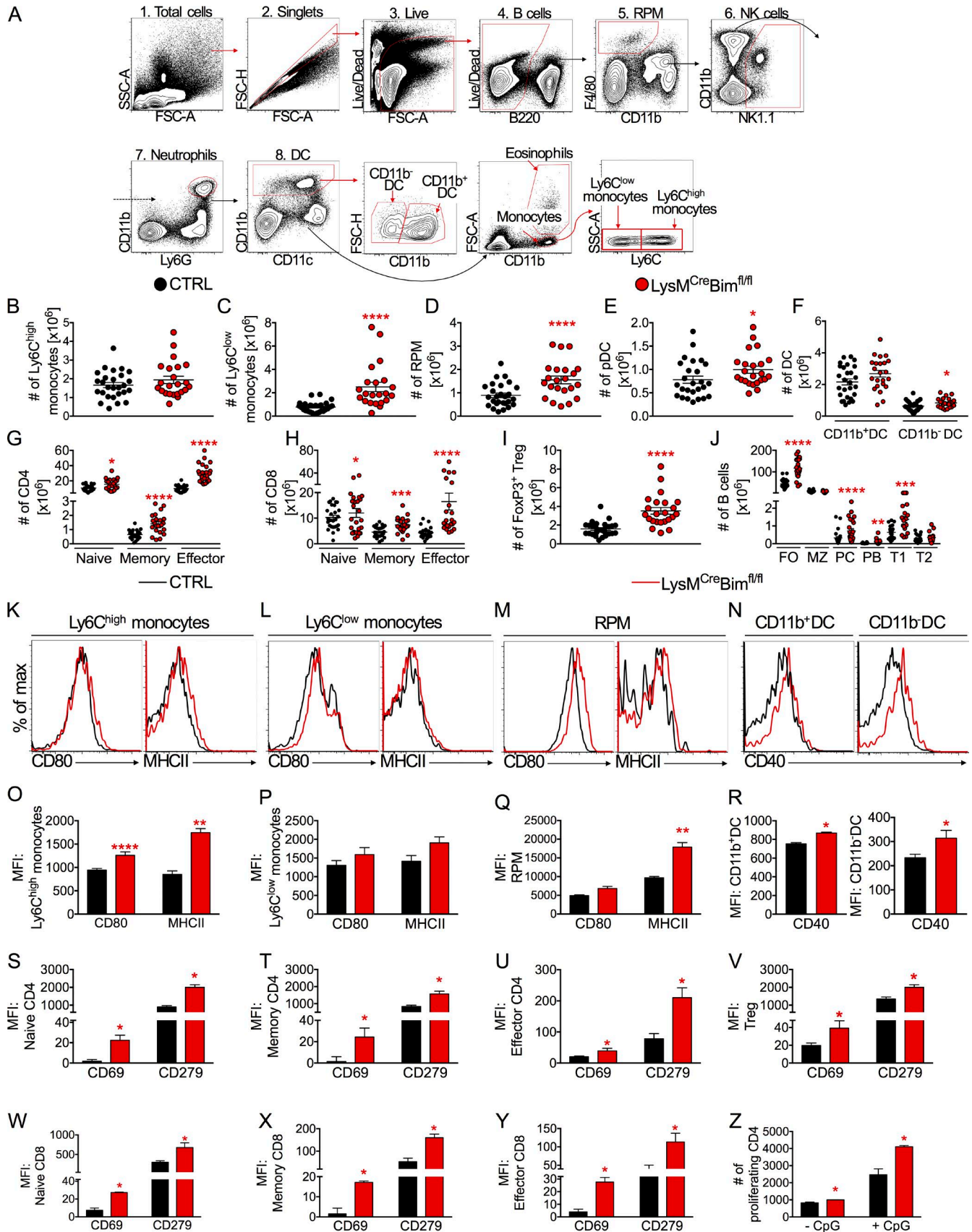


Figure 3. **LysM^{Cre}Bim^{fl/fl} mice show a loss of splenic MZMs.** (A) Representative photomicrographs of frozen spleen sections stained with B220-FITC (green, follicles) CD169-PE (red, MMMs), and CD209b-APC (pink, MZMs). Bars, 20 μ m. (B–E) Quantitative analysis of splenic MZMs and MMMs in CTRL ($n \geq 5$) and LysM^{Cre}Bim^{fl/fl} ($n \geq 5$) mice showing the number of CD11b⁺ MZMs (B), CD11b⁻ MZMs (C), CD11b⁺ MMMs (D), and CD11b⁻ MMMs (E). Data were obtained from indicated number of mice in three individual experiments and are presented as mean \pm SEM. Data were compared by Mann-Whitney test, and asterisks indicate a significant difference between LysM^{Cre}Bim^{fl/fl} and CTRL (*, $P < 0.05$; **, $P < 0.01$; ***, $P < 0.001$; ****, $P < 0.0001$). (F) Pairwise correlation matrix of gene expression between replicates of CD11b⁻ MZMs and CD11b⁺ MZMs from CTRL and LysM^{Cre}Bim^{fl/fl} mice. (G and H) Volcano plots of genes differentially expressed in CTRL and LysM^{Cre}Bim^{fl/fl} CD11b⁺ MZMs (G; $n = 2$) and CD11b⁻ MZMs (H; $n = 2$). Significantly regulated genes are indicated in color.

(Fig. 6 E). To further identify a potential apoptotic function for Bim, TUNEL analysis was performed. The number of TUNEL+ cells in 3- and 8-mo control and LysM^{Cre}Bim^{fl/fl} spleens was comparable (Fig. S4, A, C, and D). Similarly, there was no difference in the number of TUNEL+ cells in the tubular regions of 3- and 8-mo LysM^{Cre}Bim^{fl/fl} kidneys (Fig. S4, B, E, and F). In contrast, loss of Bim significantly affected the survival of bone marrow-derived macrophages (BMDMs) after growth factor withdrawal for 96 h (Fig. S4, G and H). These data suggest that Bim may have apoptotic function in an in vitro cell model, but its in vivo apoptotic function may be less evident.

The BH3 domain of Bim has been implicated in the induction of apoptosis. A previous study created mice where the BH3 domain of Bim was replaced with the domain from other BH3-only proteins such as Bad (Bim^{Bad}) and Puma (Bim^{Puma}; Mérimo et al., 2009). To examine a potential nonapoptotic function for the BH3 domain, BMDMs were treated with TLR agonists. LysM^{Cre}Bim^{fl/fl} and Bim^{Bad} BMDMs produced significantly higher levels of IL-12p40 in response to LPS or CpG treatment than controls (Fig. 6, F and G). Furthermore, Bim^{Bad} mice exhibited higher spleen weight and developed worse kidney pathology than controls (Fig. S4, I and J), whereas Bim^{Puma} mice were similar to con-



trols (Fig. 6, F and G; and Fig. S4, I and J). We then generated mice that express one Bim-BH3 mutant allele and one floxed Bim allele by crossing Bim^{Puma} , Bim^{Bad} or Bim^{Noxa} mice to $LysM^{Cre}Bim^{fl/fl}$ mice. $LysM^{Cre}Bim^{fl/+}$ and $LysM^{Cre}Bim^{fl/Puma}$ mice exhibited splenic weight and cell numbers (Fig. 6, H and I), ANA (Fig. 6, J and K), and kidney pathology (Fig. 6, N and O) comparable with controls. In contrast, $LysM^{Cre}Bim^{fl/Bad}$ and $LysM^{Cre}Bim^{fl/Noxa}$ mice displayed splenomegaly, increased ANA, and severe GN similar to $LysM^{Cre}Bim^{fl/fl}$ mice (Fig. 6, H, I, and L–O).

Deletion of TRIF ameliorates GN in $LysM^{Cre}Bim^{fl/fl}$ mice

The TLR pathway has been implicated in the development of SLE-like disease in mice (Baccala et al., 2007; Kim et al., 2009; Nickerson et al., 2010). MyD88 is the adaptor protein for most TLRs, except TLR3 and, in some cases, TLR4, which signal through TIR-domain-containing adapter-inducing IFN- β (TRIF). Therefore, we deleted MyD88 in myeloid cells or TRIF in all cells of $LysM^{Cre}Bim^{fl/fl}$ mice to generate $MyD88^{fl/fl}LysM^{Cre}Bim^{fl/fl}$ and $TRIF^{-/-}LysM^{Cre}Bim^{fl/fl}$ mice, respectively. Both $MyD88^{fl/fl}LysM^{Cre}Bim^{fl/fl}$ and $TRIF^{-/-}LysM^{Cre}Bim^{fl/fl}$ mice exhibited splenomegaly (Fig. 7, A and B) and loss of MZMs (Fig. 7 C). Further, $MyD88^{fl/fl}LysM^{Cre}Bim^{fl/fl}$ (Fig. 7 D) and $TRIF^{-/-}LysM^{Cre}Bim^{fl/fl}$ mice (Fig. 7 E) showed higher titers of IgG ANA to ssDNA, dsDNA, histones, and nucleosomes and evidence of IgG-immune complex deposition in glomeruli than controls (Fig. 7 F).

Deletion of TRIF, but not MyD88, prevented GN in $LysM^{Cre}Bim^{fl/fl}$ mice (Fig. 7, G and H). We then analyzed the immune cell composition of the kidney from normal mice under steady-state conditions using multiparameter flow cytometry. Macrophages in the kidney were denoted by $CD11b^{int}CD64^{high}F4/80^{high}MHCII^{+}$ (Fig. 7 I). There were significantly higher numbers of $Ly6C^{low}$ monocytes and macrophages in the kidneys of $LysM^{Cre}Bim^{fl/fl}$ mice than in control kidneys (Fig. 7, K and L). However, the number of $Ly6C^{high}$ monocytes and macrophages was significantly lower in $TRIF^{-/-}LysM^{Cre}Bim^{fl/fl}$ mice than $LysM^{Cre}Bim^{fl/fl}$ mice (Fig. 7, J and L). To further identify whether TRIF signaling is enhanced in $LysM^{Cre}Bim^{fl/fl}$ mice, we treated BMDMs with

poly(I:C). There was a dramatic increase of IRF3 and TBK1 phosphorylation/activation in $LysM^{Cre}Bim^{fl/fl}$ BMDMs compared with controls (Fig. S5 A). In contrast, LPS stimulation had no effect on IRF3/TBK1 activation (Fig. S5 A) but induced IL-12 and TNF production (Fig. S5 B).

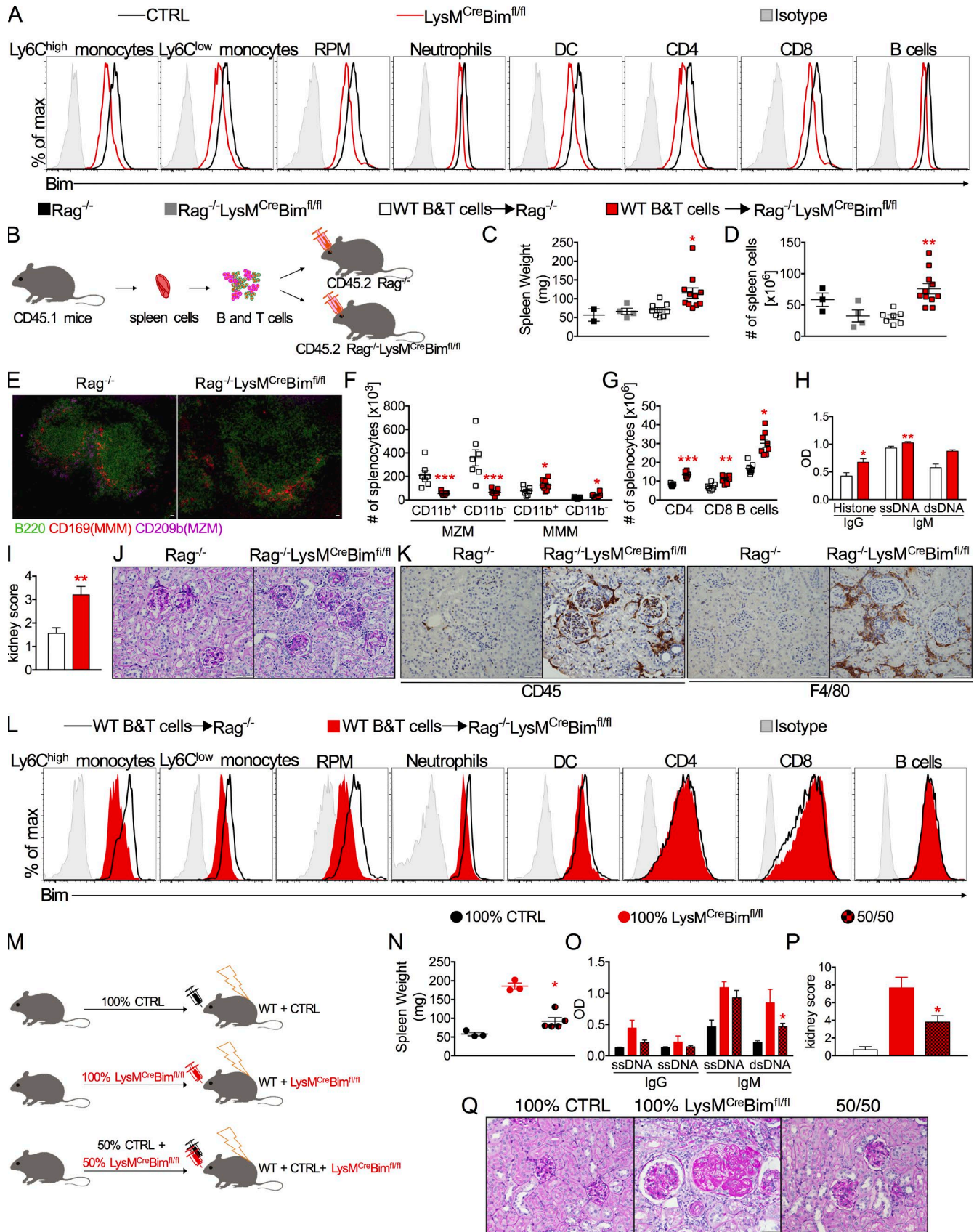
$LysM^{Cre}Bim^{fl/fl}$ mice display an SLE-like specific transcriptional signature

We performed RNA-seq of kidney macrophages ($CD11b^{int}CD64^{high}$) from control and $LysM^{Cre}Bim^{fl/fl}$ mice to study the transcriptional response in kidney macrophages. We found 87 significantly up-regulated and 69 significantly down-regulated genes in $LysM^{Cre}Bim^{fl/fl}$ kidney macrophages compared with controls (Fig. 8 A). GO enrichment analysis revealed that the up-regulated genes, such as *Nod1*, *Cd84*, and *Cd274*, are involved in “regulation of immune system process” (false discovery rate [FDR] adjusted $P = 6.66 \times 10^{-2}$; Fig. 8 B), whereas the down-regulated genes, such as *Hdac9*, *Cd36*, and *Adrb2*, are enriched for “regulation of vasculature development” (Fig. 8 B). K-means clustering ($K = 4$; Fig. 8 C) of the 5,694 differentially expressed genes (fold change ≥ 1.5 , compared across any two of the strains) yielded three main categories: genes that were regulated by both Bim and TRIF are denoted in cluster I (lupus nephritis [LN] signature), genes that were affected by Bim independent of TRIF are indicated in cluster II (Bim-regulated signature), and genes that were regulated by TRIF independent of Bim are expressed in clusters III and IV (TRIF-regulated genes). Next, we verified that the overlap of genes regulated by both Bim and TRIF (cluster I, LN signature) did not occur by chance (Fig. 8 D). We found that the number of genes demonstrating reverse regulation between control to $LysM^{Cre}Bim^{fl/fl}$ kidney macrophages and $LysM^{Cre}Bim^{fl/fl}$ to $TRIF^{-/-}LysM^{Cre}Bim^{fl/fl}$ kidney macrophages was higher than expected (χ^2 test, $P < 10^{-110}$; Fig. 8 E).

$LysM^{Cre}Bim^{fl/fl}$ kidney macrophages share a common transcriptional signature with Bim-deleted MZMs, NZB/W kidney macrophages, and human LN kidneys

We then calculated the number of differential genes as a result of Bim deletion across the affected tissues by ex-

Figure 4. **Macrophages exhibit an increased activation status and induce a hyperactive lymphocyte phenotype in $LysM^{Cre}Bim^{fl/fl}$ mice.** (A) Gating strategy used to identify monocytes macrophages and DCs in the spleen. (B–J) Quantitative analysis of $Ly6C^{high}$ monocytes (B); $Ly6C^{low}$ monocytes (C); red-pulp macrophages (D; RPM); plasmacytoid DCs (E; pDC; $CD11c^{int}PDCA-1^{+}B220^{+}$); $CD11b^{+}$ and $CD11b^{-}$ DCs (F); $CD4^{+}$ (G) and $CD8$ naive (H; $CD44^{-}CD62L^{+}$), memory ($CD44^{+}CD62L^{+}$), and effector ($CD44^{+}CD62L^{-}$) T cells (H); regulatory T cells (I; $CD4^{+}CD25^{+}Foxp3^{+}$); and B cell subsets (J; follicular [FO], $CD19^{+}CD21/35^{+}CD23^{+}$; marginal zone cells [MZ], $CD19^{+}CD21/35^{+}CD23^{low}$; plasma cells [PC], $CD19^{+}B220^{high}CD138^{+}CD21/35^{-}CD23^{-}$; plasmablasts [PB], $CD19^{+}B220^{low}CD138^{+}CD21/35^{-}CD23^{-}$, transitional 1 [T1] $B220^{+}AA4.1^{+}CD23^{-}$, and transitional 2 [T2] $B220^{+}AA4.1^{+}CD23^{+}$; CTRL, $n \geq 20$, $LysM^{Cre}Bim^{fl/fl}$, $n \geq 19$). (K–R) Quantitative analysis of expression of CD80 and MHCII or CD40 on $Ly6C^{high}$ monocytes (K and O), $Ly6C^{low}$ monocytes (L and P), RPM (M and Q), and $CD11b^{+}$ and $CD11b^{-}$ DCs (N and R; CTRL, $n \geq 4$ and $LysM^{Cre}Bim^{fl/fl}$, $n \geq 6$). (S–Y) Quantitative analysis of expression of CD69 and CD279 on T cell populations, including naïve (S and W), memory (T and X), and effector (U and Y) $CD4^{+}$ and $CD8^{+}$ T cells and regulatory T cells (V; CTRL, $n \geq 4$ and $LysM^{Cre}Bim^{fl/fl}$, $n \geq 5$). Data were obtained from the indicated number of mice in six individual experiments. Data are presented as mean \pm SEM and were compared by Mann-Whitney test, and asterisks indicate a significant difference between $LysM^{Cre}Bim^{fl/fl}$ and CTRL (*, $P < 0.05$; **, $P < 0.01$; ***, $P < 0.001$; ****, $P < 0.0001$). (Z) Purified $CD11b^{+}$ macrophages and DCs from CTRL ($n = 3$) and $LysM^{Cre}Bim^{fl/fl}$ ($n = 3$) mice were pulsed with OVA and cultured with OT-II $CD4^{+}$ T cells. Representative data from two independent experiments are presented as mean \pm SD and were compared by Student's *t* test. Asterisk indicates a significant difference between $LysM^{Cre}Bim^{fl/fl}$ and CTRL mice (*, $P < 0.05$). MFI, mean fluorescence intensity.



amining $\text{LysM}^{\text{Cre}}\text{Bim}^{\text{fl/fl}}$ CD11b^+ MZMs, CD11b^- MZMs, and kidney macrophages (Fig. 3, G and H; and Fig. 8 A). Significant numbers of genes from CD11b^+ MZMs (two genes, $P < 10^{-2}$) and CD11b^- MZMs (three genes, $P < 0.05$) overlapped with kidney macrophages (Fig. 9 A and Table S2). Additionally, CD11b^- MZMs shared a significant number of genes with CD11b^+ MZMs (two genes, $P < 10^{-3}$; Fig. 9 A and Table S2). We also compared our results to a microarray dataset from a previously published mouse model of lupus (Berthier et al., 2012), which examined kidney macrophages from young and old NZB/W mice. We identified a strong positive correlation ($R = 0.63$) in gene expression profiles between $\text{LysM}^{\text{Cre}}\text{Bim}^{\text{fl/fl}}$ kidney macrophages and NZB/W kidney macrophages (Fig. 9 B). Additionally, we compared our results to a microarray dataset from whole kidney biopsy specimens from human LN patients separated into tubulointerstitial or glomerular compartments (Berthier et al., 2012). $\text{LysM}^{\text{Cre}}\text{Bim}^{\text{fl/fl}}$ kidney macrophages and tubulointerstitial and/or glomerular tissue of human LN demonstrated a low but positive correlation ($R = 0.1$; Fig. 9, C and D). There were 33 genes (22 up- and 11 down-regulated; Table S3) in common between $\text{LysM}^{\text{Cre}}\text{Bim}^{\text{fl/fl}}$ kidney macrophages and NZB/W kidney macrophages ($P < 10^{-4}$; Fig. 9 E). These genes were enriched for GO processes such as “adaptive immune response” (FDR adjusted $P = 6.03 \times 10^{-2}$), “positive regulation of mononuclear cell migration” (FDR adjusted $P = 1.13 \times 10^{-1}$), and “negative regulation of IL-10 production” (FDR adjusted $P = 9.63 \times 10^{-2}$). The kidney macrophages from $\text{LysM}^{\text{Cre}}\text{Bim}^{\text{fl/fl}}$ mice shared a significant number of genes with the tubulointerstitial area (seven genes, $P < 10^{-2}$; Fig. 9 F and Table S3) but shared only five genes with glomerular tissue (Fig. 9 F). The five shared genes from tubulointerstitial and glomerular area of human LN included *ISG15*, *LY6E*, *LYZ*, *MS4A6A*, and *IFITM3* (Table S3). Collectively, these data suggest that the loss of Bim in myeloid cells leads to systemic autoimmunity and end-stage GN. Thus, $\text{LysM}^{\text{Cre}}\text{Bim}^{\text{fl/fl}}$ mice represent a new model of SLE that shares characteristics with established murine models of SLE-like disease and LN patients.

DISCUSSION

The origin of the break in tolerance leading to development of SLE and subsequent GN is unknown. Previous studies suggested that the Bcl-2 family members may be critical for this process. $\text{Bim}^{-/-}$ and mice lacking Bim in all hematopoietic cells ($\text{Vav}^{\text{Cre}}\text{Bim}^{\text{lox/lox}}$) develop systemic autoimmunity and end-stage LN (Bouillet et al., 2002; Herold et al., 2014). Only $\text{CD19}^{\text{Cre}}\text{Bax}^{\text{fl/-}}\text{Bak}^{-/-}$, $\text{Bax}^{-/-}\text{Bak}^{-/-}$ chimeras or vav-Bcl-2-tg mice exhibit a systemic autoimmune disease phenotype similar to $\text{Bim}^{-/-}$ mice (Takeuchi et al., 2005; Mason et al., 2013). Here, we examine the impact of deleting Bim in the myeloid cell compartment using $\text{LysM}^{\text{Cre}}\text{Bim}^{\text{fl/fl}}$ mice. $\text{LysM}^{\text{Cre}}\text{Bim}^{\text{fl/fl}}$ mice display hallmarks of SLE-like disease, including loss of MZMs, splenomegaly, lymphadenopathy, autoantibody production, IFN signature, and increased mortality. However, further analysis reveals promiscuity in the LysM promoter, consistent with previous studies that suggested LysM may be expressed not only in myeloid cells but also in developing hematopoietic cells that differentiate into B and T cells (Miyamoto et al., 2002; Ye et al., 2003). Interestingly, Fas and caspase-8 deletion is intact in lymphocytes from $\text{LysM}^{\text{Cre}}\text{Fas}^{\text{fl/fl}}$ and $\text{LysM}^{\text{Cre}}\text{caspase-8}^{\text{fl/fl}}$ mice, respectively (Cuda et al., 2012, 2015). These data suggest that the leakiness of LysM may be more dependent on the accessibility of the floxed gene. Nonetheless, studies using $\text{Rag}^{-/-}\text{LysM}^{\text{Cre}}\text{Bim}^{\text{fl/fl}}$ mice that received adoptively transferred WT lymphocytes eliminates any possibility that the susceptibility to SLE-like disease in $\text{LysM}^{\text{Cre}}\text{Bim}^{\text{fl/fl}}$ may be derived from Bim-deleted B and T cells. However, our data do not rule out an effect of the loss of Bim in other myeloid populations such as DCs and neutrophils. As opposed to $\text{CD19}^{\text{Cre}}\text{Bax}^{\text{fl/-}}\text{Bak}^{-/-}$ mice (Takeuchi et al., 2005), $\text{CD4}^{\text{Cre}}\text{Bim}^{\text{fl/fl}}$ and $\text{CD19}^{\text{Cre}}\text{Bim}^{\text{fl/fl}}$ mice fail to develop an SLE-like disease phenotype, even though they are on an autoimmune prone background. These data suggest that Bim plays a role in autoimmunity that does not parallel other Bcl-2 proteins; furthermore, deletion of Bim in myeloid cells, including macrophages, is sufficient to induce the development of autoimmunity in mice.

Previous studies have suggested that a failure to process apoptotic bodies by MZMs, which normally induces toler-

Figure 5. Adoptive transfer of WT B and T cells into $\text{Rag}^{-/-}\text{LysM}^{\text{Cre}}\text{Bim}^{\text{fl/fl}}$ mice is sufficient to cause SLE-like disease. (A) Representative histograms of Bim expression in hematopoietic cells in CTRL ($n = 3$) and $\text{LysM}^{\text{Cre}}\text{Bim}^{\text{fl/fl}}$ mice ($n = 4$). Data are from three independent experiments. RPM, red-pulp macrophage. (B) Representation of experimental design as described in Materials and methods. (C and D) Quantitative analysis of spleen weights (C) and total live spleen cells (D). Representative photomicrographs of splenic MZMs and MZMs (E). Bars, 20 μm . (F and G) Flow cytometric analysis of MZMs and MMMs (F) and CD4, CD8 T cells and B cells (G). (H) IgG and IgM ANA titers. (I) Kidney sections scored for kidney damage. (J) Representative photomicrographs of PAS-stained kidney sections. Bars, 50 μm . (K) Representative photomicrographs of kidney sections stained with anti-CD45 and anti-F4/80 antibodies. Bars, 50 μm . (L) Representative histograms of Bim expression in hematopoietic cells in $\text{Rag}^{-/-}\text{LysM}^{\text{Cre}}\text{Bim}^{\text{fl/fl}}$ and $\text{Rag}^{-/-}$ mice receiving WT lymphocytes. Representative data from two independent experiments are shown (WT B and T cells \rightarrow $\text{Rag}^{-/-}$ mice, $n \geq 7$, WT B and T cells \rightarrow $\text{Rag}^{-/-}\text{LysM}^{\text{Cre}}\text{Bim}^{\text{fl/fl}}$, $n \geq 8$). Data are presented as mean \pm SEM and were compared by Mann-Whitney test. Asterisks indicate a significant difference between WT B and T cells \rightarrow $\text{Rag}^{-/-}\text{LysM}^{\text{Cre}}\text{Bim}^{\text{fl/fl}}$ versus WT B and T cells \rightarrow $\text{Rag}^{-/-}$ mice (*, $P < 0.05$; **, $P < 0.01$; ***, $P < 0.001$). (M) Representation of experimental design for mixed bone marrow chimeras as described in Materials and methods. (N) Splenomegaly. (O) Titers of IgG and IgM ANA. (P) Pathology score for GN from mixed bone marrow chimeras. (Q) Representative photomicrographs of PAS-stained kidney sections. Bars, 50 μm . Representative data from two independent experiments are shown (100% CTRL, $n = 3$, 100% $\text{LysM}^{\text{Cre}}\text{Bim}^{\text{fl/fl}}$, $n = 5$, 50/50, $n = 3$). Data are presented as mean \pm SEM and were compared by Mann-Whitney test. Asterisk indicates a significant difference between 100% CTRL and 50/50 (*, $P < 0.05$).

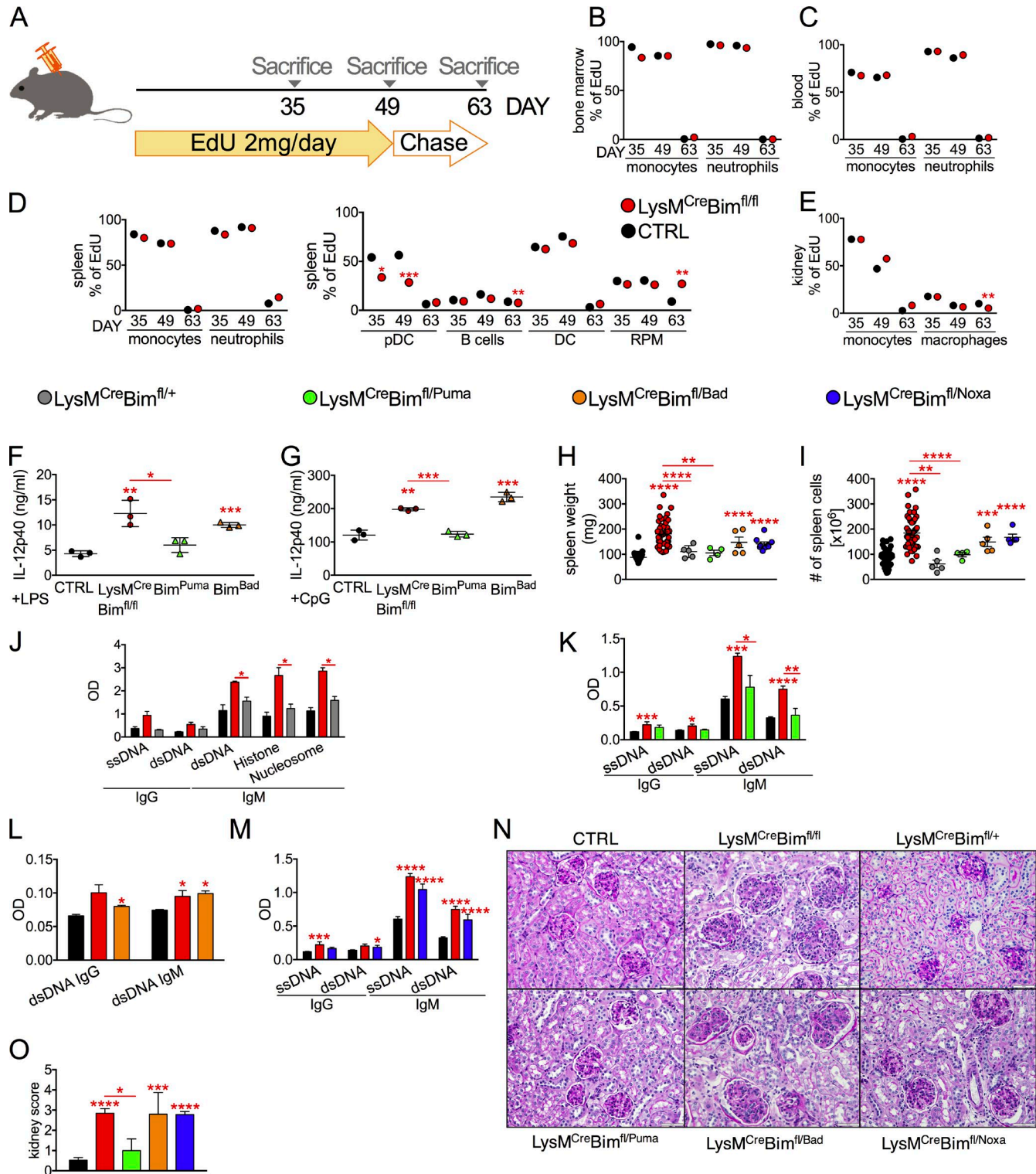


Figure 6. The systemic autoimmunity in $LysM^{Cre}Bim^{fl/fl}$ mice may not require enhanced survival of monocytes/macrophages. (A) Representation of experimental design for EdU study as described in Materials and methods. (B–E) FACS analysis of percentage of EdU incorporation in multiple immune cell populations from CTRL and $LysM^{Cre}Bim^{fl/fl}$ mice at day 35 ($n = 4$), 49 ($n \geq 8$), and 63 ($n = 6$) in bone marrow (B), blood (C), spleen (D), and kidney (E). The experiment was performed one time. Data are presented as mean \pm SEM and were compared by Mann–Whitney test. Asterisks indicate a significant difference between $LysM^{Cre}Bim^{fl/fl}$ and CTRL (*, $P < 0.05$; **, $P < 0.01$; ***, $P < 0.001$). (F and G) Bim^{Bad} GM-CSF BMDMs were hyperresponsive to TLR activation. BMDMs were stimulated with either LPS (F) or CpG (G) for 6 h, and supernatants were collected and evaluated for IL-12p40 by multiplex immunoassay as

ance, may be necessary for the activation of lymphocytes in SLE-like disease (McGaha and Karlsson, 2016). We observe that the MZMs are absent as early as 1.5 mo of age in $LysM^{Cre} Bim^{fl/fl}$ mice, whereas the numbers or topography of the MMMs are minimally affected. Similarly, $Rag^{-/-}LysM^{Cre} Bim^{fl/fl}$ mice reconstituted with WT lymphocytes also exhibit a reduced number of MZMs, whereas the MZMs in $Rag^{-/-}$ mice transferred with WT lymphocytes are normal. The increased numbers of pDCs in the spleen are associated with elevated serum levels of type I IFN in $LysM^{Cre}Bim^{fl/fl}$ mice. These data are consistent with a recent study, which suggested that the lack of MZMs may be because of the recruitment of type I IFN-expressing pDCs. Further, type I IFN alters the location of MZB cells, thereby disrupting the lymphotoxin signaling pathway in MZMs (Li et al., 2015). In line with this, we detected a change in the localization of MZB cells but not in their total number in $LysM^{Cre}Bim^{fl/fl}$ mice. However, we did not observe any difference in the gene expression of the members of lymphotoxin pathway, including megakaryoblastic leukemia 1, megakaryoblastic leukemia 2, and serum response factor (Li et al., 2015). Although our study has some limitations, the differences in lymphotoxin pathway gene expression between the previous model and $LysM^{Cre}Bim^{fl/fl}$ mice may be because of the numbers of replicates or the lupus models being investigated.

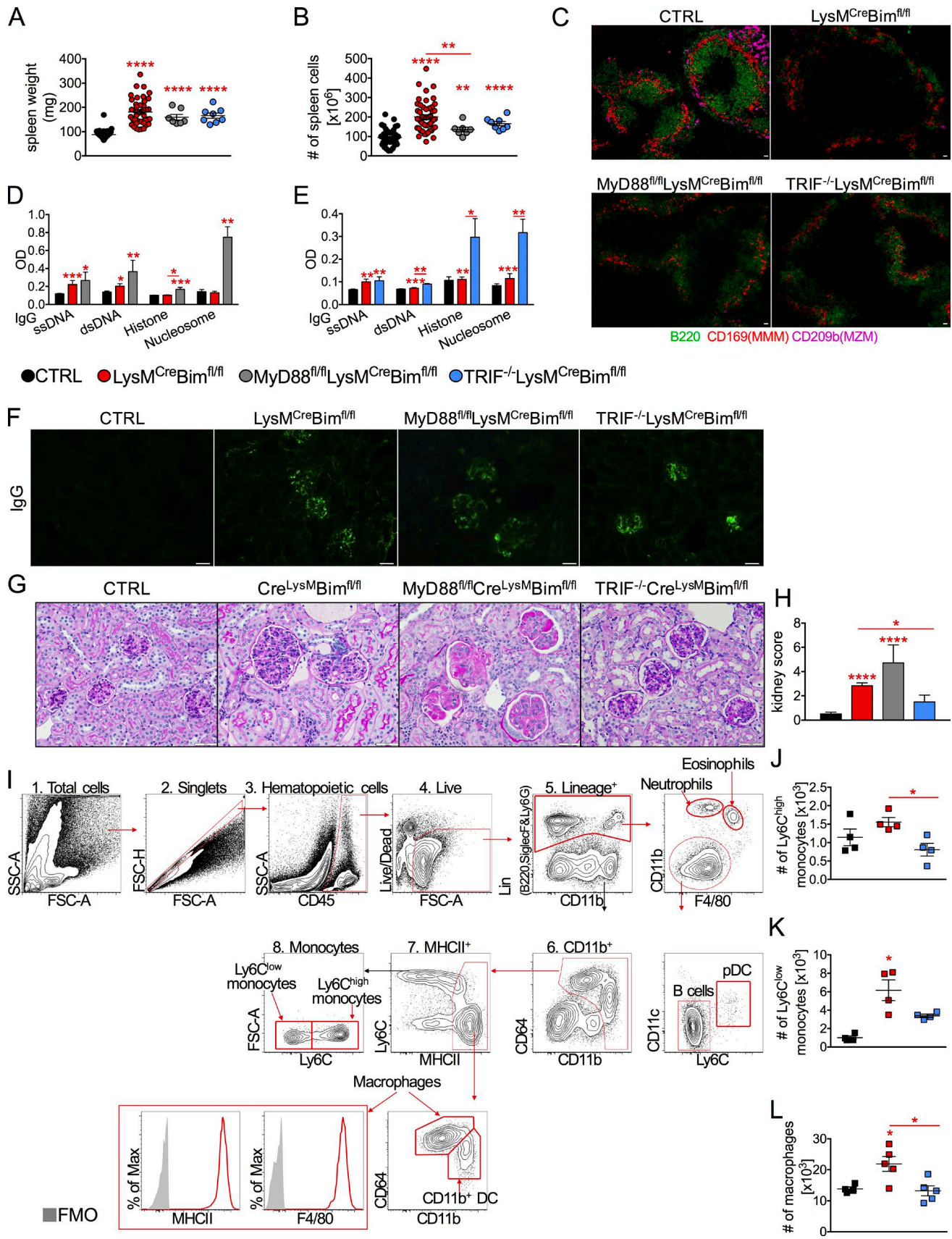
Although Bim is crucial for maintaining hematopoietic cell homeostasis through the induction of apoptotic cell death, our data suggest that Bim may also play a nonapoptotic role that affects the development of SLE-like disease. These data are also consistent with previous studies suggesting that the Bcl-2 pathway, including Bim, may have nonapoptotic functions in macrophages and DCs (Nopora and Brocker, 2002; Hou and Van Parijs, 2004; Chen et al., 2007; Gautier et al., 2008; Hutcheson and Perlman, 2008; Hutcheson et al., 2008; Scatizzi et al., 2010; Yeretssian et al., 2011). We show that Bim-deleted macrophages display increased markers of activation and secrete elevated levels of cytokines, and these results are similar to those of our previous study (Scatizzi et al., 2010). Loss of Bim has no effect on the turnover of MZMs or even in development of MZMs in the $Rag^{-/-}$ background. Additionally, pulse-chase EdU studies suggest that Bim either reduces the rate of proliferation or has only a minor effect on the cell death of myeloid cells. However, because we do not observe a difference in the rate of EdU uptake, these data would suggest that the rate of proliferation is the same

in monocytes and macrophages regardless of the presence of Bim. We cannot rule out that there is a marginal effect on apoptosis, because Bim-deleted BMDMs have lower levels of apoptosis than controls.

Previous studies have shown that the BH3 protein family is divided into direct and indirect activators of cell death. Bid, Bim, and Puma are considered activators of apoptosis, as BH3 peptides from these proteins are capable of inducing apoptosis (Billard, 2013). Macrophages from Bim^{Bad} and $LysM^{Cre}Bim^{fl/fl}$, but not Bim^{Puma} mice, exhibit enhanced cytokine production in response to TLR stimulation that is independent of cell death. Further, replacement of one of the Bim alleles in $LysM^{Cre}Bim^{fl/fl}$ mice with that of Bad- or Noxa-BH3 leads to an SLE-like disease that mirrors $LysM^{Cre}Bim^{fl/fl}$ mice. In contrast, replacement of Bim-BH3 with Puma-BH3 prevents SLE-like disease and resembles WT or $LysM^{Cre}Bim^{fl/+}$ mice. These data are consistent with the notion that the BH3 domain of Puma may function in a manner similar to the BH3 domain of Bim (Mérino et al., 2009). Our data partially agree with the study demonstrating that Bim^{Bad} or Bim^{Noxa} rescues the lethal disease seen in $Bcl-2^{-/-}$ mice (Mérino et al., 2009). Differences between the studies may reflect the mechanism of disease (i.e., $Bcl-2^{-/-}$ mice develop hematopoietic deficiency and PKD, whereas $LysM^{Cre}Bim^{fl/fl}$ mice develop systemic autoimmunity and LN). Collectively, these data suggest that the BH3 domain of Bim in myeloid cells is required to suppress systemic autoimmunity. Moreover, Bim may have multiple functions in myeloid cells that can contribute to SLE-like disease. Future studies are required to definitively show that Bim has a direct nonapoptotic function.

Our cell culture data using BMDMs suggest that the loss of Bim may enhance TLR signaling. However, deletion of MyD88 or TRIF in $LysM^{Cre}Bim^{fl/fl}$ mice has no effect on systemic autoimmunity. In contrast, loss of TRIF in $LysM^{Cre}Bim^{fl/fl}$ mice is sufficient to suppress the progression to full-blown GN. Although $TRIF^{-/-}LysM^{Cre}Bim^{fl/fl}$ mice display immune complex deposition, there is limited macrophage infiltrate and reduced GN. These data suggest that macrophage infiltration is necessary for the destruction of the kidney, consistent with human studies (Hill et al., 2001). The deletion of TRIF in $LysM^{Cre}Bim^{fl/fl}$ mice clearly delineates systemic autoimmunity from end-organ disease, consistent with a previous study (Ge et al., 2013). Our cell culture studies using BMDMs suggest that loss of Bim leads to enhanced TBK1 activation in response to TLR3 signaling, which occurs

described in Materials and methods ($n = 3$). Representative data from three independent experiments are shown. Data are presented as mean \pm SD and were compared by Student's *t*-test. Asterisks indicate a significant difference between $LysM^{Cre}Bim^{fl/fl}$ or Bim^{Bad} and CTRL (*, $P < 0.05$; **, $P < 0.01$; ***, $P < 0.001$). (H-O) 8-mo-old female CTRL ($n \geq 27$), $LysM^{Cre}Bim^{fl/fl}$ ($n \geq 17$), $LysM^{Cre}Bim^{fl/+}$ ($n = 5$), $LysM^{Cre}Bim^{fl/Puma}$ ($n \geq 3$), $LysM^{Cre}Bim^{fl/Bad}$ ($n \geq 3$), and $LysM^{Cre}Bim^{fl/Noxa}$ ($n = 9$) mice were examined for systemic autoimmune disease. Quantitative analysis of spleen weights (H) and total live spleen cells (I). Serum was measured for titers of IgG and IgM ANA(U-M). (N) Representative photomicrographs of PAS-stained kidney sections. Bars, 50 μ m. (O) Kidney sections scored for kidney damage. Data were obtained from the indicated number of mice in three individual experiments. Data are presented as mean \pm SEM and were compared by Mann-Whitney test. Asterisks indicate a significant difference between $LysM^{Cre}Bim^{fl/fl}$, $LysM^{Cre}Bim^{fl/Bad}$ or $LysM^{Cre}Bim^{fl/Noxa}$ and CTRL (*, $P < 0.05$; **, $P < 0.01$; ***, $P < 0.001$; ****, $P < 0.0001$).



through TRIF. Future studies may require generating $LysM^{Cre} Bim^{fl/fl}$ mice that also lack TBK1. However, we cannot rule out that TRIF-deleted kidney stromal cells or other nonmyeloid cells influence macrophage recruitment. Although loss of MyD88 exacerbates the development of LN in $LysM^{Cre} Bim^{fl/fl}$ mice, this altered phenotype may be caused by overcompensation by the TRIF signaling pathway. Because both MyD88 and TRIF are involved in downstream signaling for TLR4, future studies are necessary to examine the role that TLR4 pathway plays in disease. Our data are novel and are in contrast with other studies showing that MyD88 deletion is required in B cells and DCs to prevent systemic autoimmunity in $Lyn^{-/-}$ mice (Ban et al., 2016) and for the expansion of lymphocytes and end-organ damage in MRL/lpr mice (Teichmann et al., 2010). Differences between our data and those using $Lyn^{-/-}$ and MRL/lpr mice may be attributed to background of the mice and the affected cells caused by global gene deficiency.

Numerous studies have used gene expression profiling of peripheral blood mononuclear cells and whole kidney tissue from SLE patients to gain insights into the pathobiology of disease or identification of a potential biomarker (Tsokos et al., 2016). Nonetheless few studies isolated individual cell populations to understand their specific roles in SLE disease pathogenesis. Our global gene expression studies demonstrate a lupus-specific as well as a TRIF- and Bim-specific signature in kidney macrophages from control, $LysM^{Cre} Bim^{fl/fl}$, and $TRIF^{-/-} LysM^{Cre} Bim^{fl/fl}$ mice. For example, the expression level of CD36, a receptor known to be involved in phagocytosis of apoptotic bodies, is lower in $LysM^{Cre} Bim^{fl/fl}$ kidney macrophages than control kidney macrophages. Expanding our analysis to MZMs from $LysM^{Cre} Bim^{fl/fl}$ mice yields some commonalities. We also identify similarities between kidney macrophage transcriptional signatures in $LysM^{Cre} Bim^{fl/fl}$ mice and those from old NZB/W mice, even though these cells are from two different backgrounds. Of note, both *Cd274* (PD-L1; Dai et al., 2014) and *Ccl2* (Tesch et al., 1999), known contributors to SLE, are enhanced in these cells. Additionally, we detected a significant number of overlapping genes between tubulointerstitial tissue of LN patients and kidney macrophages from $LysM^{Cre} Bim^{fl/fl}$ mice. Despite the difficulties of comparing transcriptional signatures across species and techniques (RNA-seq vs. microarray), seven genes are shared between $LysM^{Cre} Bim^{fl/fl}$ kidney macrophages and tubulointer-

stitial tissue, including *IFITM2* (Rai et al., 2016), *LY6E*, and *ISG15* (Feng et al., 2006), genes known to be highly expressed in SLE patients. However, given that the patient data represent whole tissue, it is unknown whether the increased expression in these genes from the lupus patient datasets is macrophage specific. Future studies require a direct comparison of isolated macrophages from kidneys of SLE patients with those from murine studies. Collectively, we have established a novel model of SLE-like disease that is mediated by loss of Bim in myeloid cells. Further, our data demonstrate that Bim is a new therapeutic target for SLE treatment.

MATERIALS AND METHODS

Mice

Mice homologous for loxP-flanked Bim allele (CTRL: $LysM^{+/+} Bim^{fl/fl}$, C57BL/6:129 mixed background) were a gift from the late S. Korsmeyer and J. Opferman (Takeuchi et al., 2005; Steimer et al., 2009) and were mated with mice expressing Cre under the control of LysM promoter ($LysM^{Cre}$; The Jackson Laboratory), CD19-Cre ($CD19^{Cre}$) knock-in mice, or CD4-Cre ($CD4^{Cre}$; Taconic Biosciences, Inc.) transgenic mice. In addition, $Bim^{fl/fl}$ were backcrossed to C57BL/6 by The Jackson Laboratory using speed congenics to achieve 98% C57BL/6. The mice were then backcrossed to C57BL/6 for two additional generations to generate congenic $Bim^{fl/fl}$ mice. After backcross, $Bim^{fl/fl}$ mice were mated with $LysM^{Cre}$ mice to generate $LysM^{Cre} Bim^{fl/fl}$. The fidelity of deleting Bim in $LysM^{Cre} Bim^{fl/fl}$ was previously published and confirmed by us (Takeuchi et al., 2005; Steimer et al., 2009). $Rag^{-/-}$ mice (The Jackson Laboratory), $MyD88^{fl/fl}$ mice (The Jackson Laboratory), and $TRIF^{-/-}$ mice (The Jackson Laboratory) were crossed to $LysM^{Cre} Bim^{fl/fl}$ to generate $Rag^{-/-} LysM^{Cre} Bim^{fl/fl}$ mice, $LysM^{Cre} Bim^{fl/fl} MyD88^{fl/fl}$ mice, and $TRIF^{-/-} LysM^{Cre} Bim^{fl/fl}$ mice. Bim^{Bad} , Bim^{Noxa} , and Bim^{Puma} mice were provided by P. Bouillet (Mérino et al., 2009). Bim^{Bad} , Bim^{Noxa} , and Bim^{Puma} mice were crossed with $LysM^{Cre} Bim^{fl/fl}$ to generate $LysM^{Cre} Bim^{fl/fl/Bad}$, $LysM^{Cre} Bim^{fl/fl/Noxa}$, and $LysM^{Cre} Bim^{fl/fl/Puma}$ mice. $CD4^{Cre} Bim^{fl/fl}$ and $dLck^{Cre} Bim^{fl/fl}$ mice were generated on a C57BL/6 background as previously described (Herold et al., 2014; Li et al., 2017; provided by D.A. Hildeman, University of Cincinnati, Cincinnati, OH). B6 CD45.1/2 mice were generated by crossing B6 mice to B6.CD45.1 mice. All mice were housed and bred at a barrier- and specific-pathogen-free facility at the Center for Comparative Medicine at

Figure 7. MyD88 or TRIF is not required for the systemic autoimmunity but TRIF is necessary for GN in $LysM^{Cre} Bim^{fl/fl}$ mice. (A–H) 8-mo-old female CTRL ($n \geq 8$), $LysM^{Cre} Bim^{fl/fl}$ ($n \geq 9$), $MyD88^{fl/fl} LysM^{Cre} Bim^{fl/fl}$ ($n = 7$), and $TRIF^{-/-} LysM^{Cre} Bim^{fl/fl}$ ($n \geq 6$) mice were examined for splenomegaly (A and B). (C) Representative photomicrographs of splenic MZMs and MZM. Bars, 20 μm . (D and E) Titers of IgG ANA. (F) Immune complex deposition. Photomicrograph of anti-IgG-FITC-stained frozen kidney sections. Bars, 50 μm . (G) Representative photomicrographs of PAS-stained kidney sections. Bars, 50 μm . (H) Kidney scores. Data were obtained from the indicated number of mice in three individual experiments. (I) Flow cytometric gating strategy for monocytes and macrophages in the kidney FMO, fluorescence minus one. Quantitative analysis of infiltrating monocytes and macrophages in the kidneys of CTRL ($n = 4$), $LysM^{Cre} Bim^{fl/fl}$ ($n = 5$), and $TRIF^{-/-} LysM^{Cre} Bim^{fl/fl}$ ($n = 5$) mice. (J–L) Number of Ly6C^{high} monocytes (J), Ly6C^{low} monocytes (K), and macrophages (L). Representative data from three independent experiments are shown. Data are presented as mean \pm SEM and were compared by Mann-Whitney test. Asterisks indicate a significant difference between $LysM^{Cre} Bim^{fl/fl}$, $MyD88^{fl/fl} LysM^{Cre} Bim^{fl/fl}$ or $TRIF^{-/-} LysM^{Cre} Bim^{fl/fl}$ and CTRL (*, $P < 0.05$; **, $P < 0.01$; ***, $P < 0.001$; ****, $P < 0.0001$).

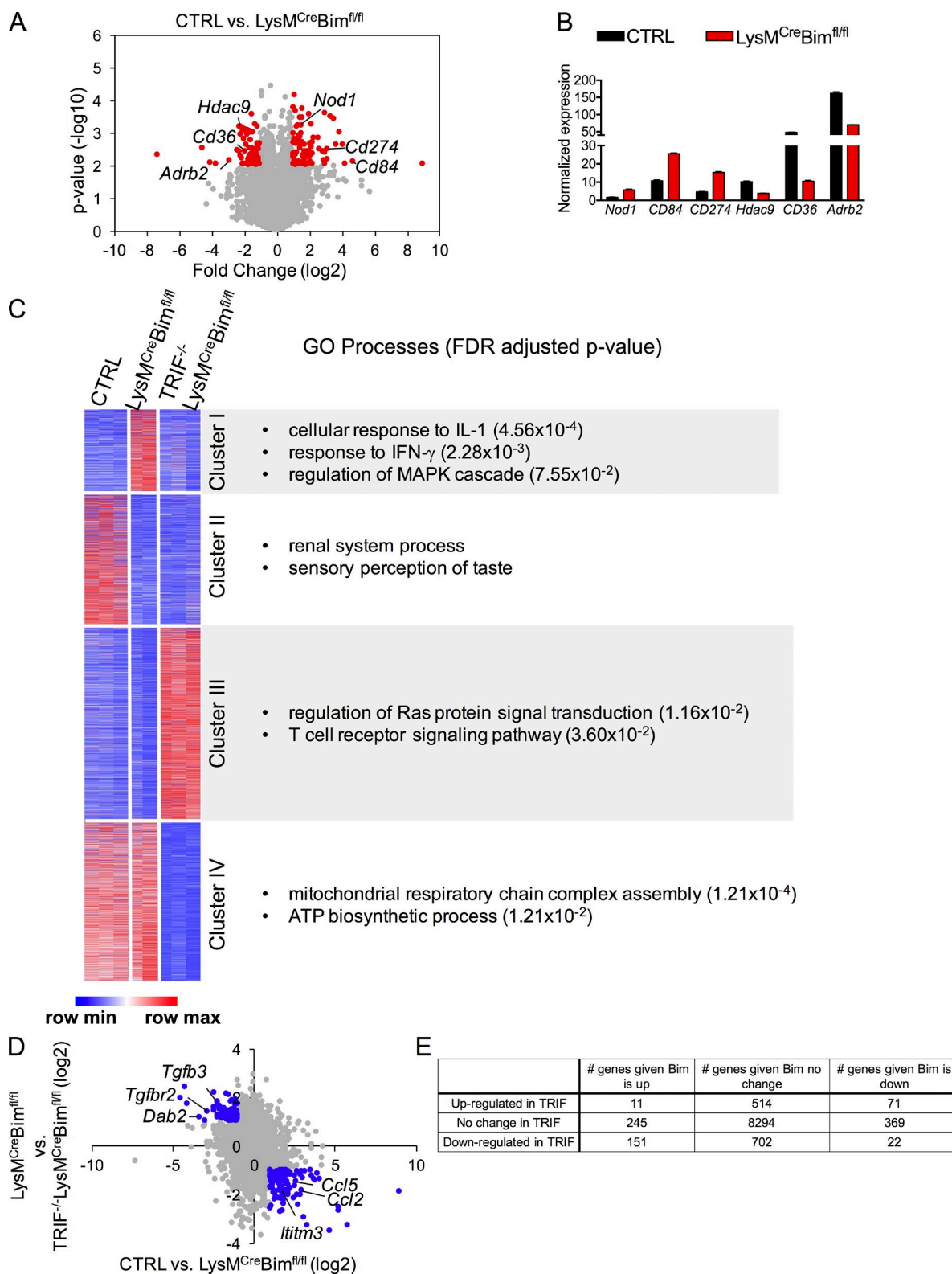


Figure 8. **Bim cooperates with TRIF to regulate transcriptional profiles of kidney macrophages.** (A) Volcano plot of differentially expressed genes in $LysM^{Cre}Bim^{fl/fl}$ kidney macrophages compared with CTRL kidney macrophages. Significantly regulated genes are indicated in red ($n = 2$). (B) Bar graphs indicating the normalized gene expression of individual genes in CTRL and $Cre^{LysM}Bim^{fl/fl}$ kidney macrophages. Data are presented as mean \pm SEM. (C) Heat map of K-means ($K = 4$) clustering on 5,694 differential genes and GO processes from each cluster. (D) Scatterplot showing fold change of gene expression

Northwestern University. Genotyping of the mice was done by Transnetyx. Female mice were used for all experiments. Proteinuria was measured with Uristix reagent strips (Siemens Healthcare Diagnostics). All housing conditions and animal experiments were approved by the Northwestern University Institutional Animal Care and Use Committee.

Histopathology and immunohistochemistry

Spleen and kidney were isolated and fixed in 2% paraformaldehyde. 4- μ m paraffin-embedded kidney and spleen sections were stained with periodic acid–Schiff base (PAS), H&E, F4/80, or CD45 as previously described (Hutcheson et al., 2008). The PAS-stained kidney sections were scored by a pathologist (G.K. Haines) blinded to the study. The kidney scores were determined by the addition of the values from glomerulosclerosis, interstitial fibrosis, and different morphological indexes based on the previous published scoring system (Hill et al., 2000). Photomicrographs were taken on an Olympus BX41 microscope equipped with an Olympus DP21 camera.

Serological tests

Serum was obtained from 8-mo-old CTRL ($Bim^{fl/fl}$) and $LysM^{Cre}Bim^{fl/fl}$ mice and was diluted 50 times in 0.1% gelatin supplemented with 2% BSA (Sigma–Aldrich), 3 mM EDTA, and 0.05% (vol/vol) Tween–20 (Sigma–Aldrich). Immulon 2 HB 96-well flat bottom plates (ImmunoChemistry Technologies) were precoated with methylated BSA followed by immobilization of antigens including dsDNA, ssDNA, histones, or dsDNA and histones (nucleosomes). Plates were washed with DPBS (Lonza) after incubation, and serum samples were added into the wells. Unbound serum samples were washed with DPBS containing 0.05% (vol/vol) Tween–20 (Sigma–Aldrich), and serum samples were conjugated to goat anti–mouse IgG or IgM antibodies conjugated with alkaline phosphatase (SouthernBiotech). pNPP (p-nitrophenyl phosphate disodium salt; Sigma–Aldrich) was used for colorimetric detection, and the plates were read at OD 405 nm on a BioTek Synergy HT Multi Mode plate reader. For measurement of serum isotyping antibodies, serum was diluted at 1:25,000, and a mouse immunoglobulin isotyping 96-well plate assay kit (EMD Millipore) was used according to the instructions of the manufacturer. The results were read on a Luminex 200 instrument running on an xPONENT software. Serum cytokines were evaluated using Luminex bead-based assays (Affymetrix).

Immunofluorescent microscopy

Kidneys were processed analysis for immune complex deposition as previously described by us (Hutcheson et al., 2008;

Cuda et al., 2014). For splenic MZMs, MMMs, and MZB cells, spleens were isolated and snap-frozen in Tissue-Tek OCT and sectioned at 8 μ m thickness followed by fixing in cold acetone and blocking with Fc Block (BD Biosciences) and normal rat serum (Jackson ImmunoResearch Laboratories). Finally, the spleen sections were stained with anti–CD209b–APC (clone REA125; Miltenyi Biotec), anti–CD169–PE (clone REA197; Miltenyi Biotec), anti–CD169–FITC (clone MOMA-1; AbD Serotec), anti–B220–Alexa Fluor 488 (clone RA3-6B2; BioLegend), anti–B220–Alexa Fluor 647 (clone: RA3-6B2; BioLegend), anti–CD1d–PE (clone 1B1; BioLegend), or anti–CD4–Alexa Fluor 647 (clone GK1.5; BioLegend). Images were acquired using a 10 \times objective on a Nikon TE2000E2–PFS running NIS–Elements software.

Tissue preparation and flow cytometry

Preparation of single-cell suspension from blood and spleen was performed as previously described (Rose et al., 2012). Kidneys were collected into cold MACS buffer (Miltenyi Biotec), carefully decapsulated, weighed, cut into small fragments (1–2 mm), and subjected to mechanically disruption using C-tubes (Miltenyi Biotec) and GentleMACS dissociator (Miltenyi Biotec) with the program *m_liver_01.02*. The disrupted kidney tissue was continuously rotated at 37°C for 30 min and subjected to GentleMACS dissociator (Miltenyi Biotec) using the program *m_liver_02.02*. Each kidney was digested with 2.5 ml in-house digestion buffer consisting of 0.76 U/ml Liberase TL (Sigma–Aldrich) and 2mg/ml DNase I (Roche) dissolved in HBSS with Ca^{2+} and Mg^{2+} (Mediatech Inc.). Cells released during enzymatic digestion were filtered through Falcon 40- μ m cell strainers (Corning), and red blood cells were lysed with Pharm Lyse Buffer (BD Biosciences). Isolated kidney cells were labeled with CD45 MicroBeads (Miltenyi Biotec) and separated on MultiMACS Cell24 Separator Plus (Miltenyi Biotec). Total numbers of live cells were counted by Countess Automated cell counter (Invitrogen), and dead cells were distinguished by Trypan Blue stain. Cells were stained with Live/Dead Aqua fluorescent dye (Invitrogen), incubated with Fc Block and then stained for 30 min with the fluorochrome-conjugated antibodies. Data were acquired on an LSR II flow cytometer (BD Biosciences). Compensation and data were analyzed using FlowJo software (Tree Star). FMO (fluorescence minus one) controls were used to gate MZM and MMM populations or when necessary. Splenic MZMs, MMMs, and kidney macrophages were sorted on a BD FACSAria SORP instrument (BD Biosciences) at the Northwestern University Robert H. Lurie Comprehensive Cancer Center Flow Cytometry Core Facility.

between CTRL and $Cre^{LysM}Bim^{fl/fl}$ kidney macrophages (x axis) and $TRIF^{-/-}Cre^{LysM}Bim^{fl/fl}$ and $Cre^{LysM}Bim^{fl/fl}$ kidney macrophages (y axis). Significantly regulated genes are indicated in blue ($n = 2$). (E) χ^2 test table examining relationship between *Bim* and *TRIF*. The number of genes differentially regulated or unchanged between CTRL and $LysM^{Cre}Bim^{fl/fl}$ kidney macrophages and $LysM^{Cre}Bim^{fl/fl}$ and $TRIF^{-/-}LysM^{Cre}Bim^{fl/fl}$ kidney macrophages from D. H_0 : *Bim* and *TRIF* are independent, H_1 : *Bim* and *TRIF* are not independent. χ^2 test ($\chi^2 > 315$) suggests a significant result ($P < 10^{-110}$).

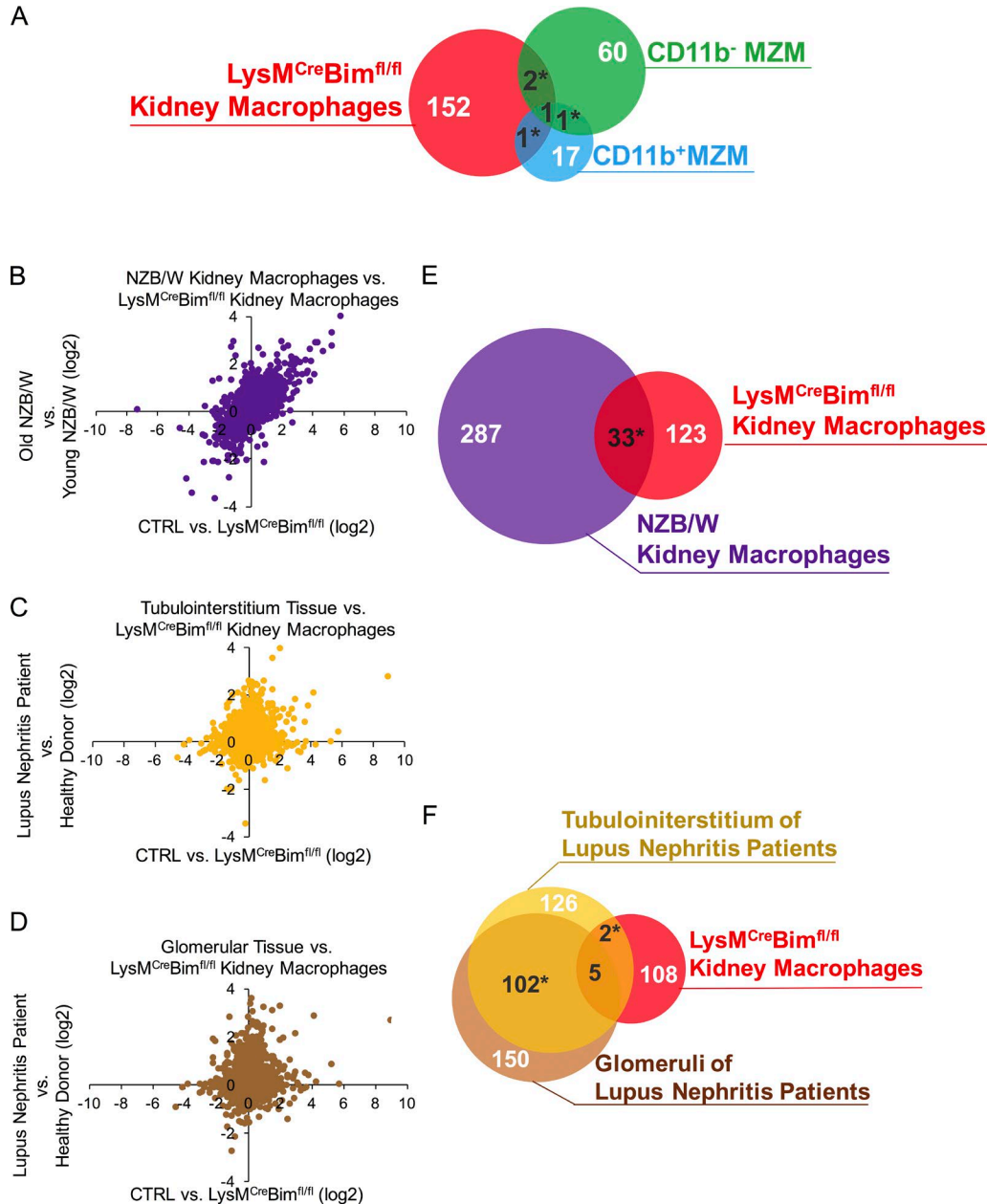


Figure 9. The deletion of Bim leads to widespread transcriptional reprogramming. (A) Venn diagram of overlap in genes from kidney macrophages ($n = 2$), CD11b⁺MZMs ($n = 2$), and CD11b⁻MZMs ($n = 2$) that are differentially expressed between CTRL and LysM^{LysM}Bim^{fl/fl} mice. Number of significantly regulated genes in kidney macrophages, CD11b⁺ MZMs, and CD11b⁻ MZMs are indicated by red, blue, and green circles, respectively. (B–D) Scatterplots show the comparison of log₂ fold change between LysM^{Cre}Bim^{fl/fl} kidney macrophages (x axis) and NZB/W kidney macrophages (B; from previously published data [Berthier et al., 2012]), tubulointerstitium of human LN (C), and glomeruli of human LN (y axis; D; from previously published data [Berthier et al., 2012]). (E) Overlap of significantly regulated genes from LysM^{Cre}Bim^{fl/fl} (red) and old NZB/W kidney macrophages (purple). A total of 320 genes were differentially expressed between young (2–6 wk before the development of terminal renal failure) and old NZB/W (8–16 wk old, $n = 6$). (F) Overlap of significantly regulated homologous genes between LysM^{Cre}Bim^{fl/fl} kidney macrophages (red), tubulointerstitium (yellow), and glomeruli (brown) of human LN. A total of 235 and 257 homologous genes were differentially expressed between human LN and living donors in tubulointerstitium ($n = 15$) and glomeruli ($n = 14$), respectively. Asterisk indicates a significant enrichment of the overlapping genes (*, $P < 0.05$).

Mixed leukocyte reaction assay

Isolation of single-cell suspension from the spleens was performed as previously described (Rose et al., 2012). In brief,

splenic CD11b⁺ cells were purified by immune-magnetic positive selection. Splenocytes were incubated with anti-CD11b MACS beads (Miltenyi Biotec), and CD11b⁺ cells were puri-

fied with a MACS column. Purity of macrophages was ~90% as determined by FACS analyses. Purified CD11b⁺ splenic cells were pulsed with 10 µg/ml OVA peptide (aa 323–339) for 60 min at 37°C in 5% CO₂. The pulsed cells were washed two times with RPMI. OVA-specific CD4 T cells were isolated from the spleens of OT-II/Rag^{-/-} mice using the CD4 T cell isolation kit (Miltenyi Biotec) according to the manufacturer's protocol. The resulting CD4 T cells were >90% purity as determined by flow cytometry. Thereafter, CD4 T cells were labeled with 500 nM CFSE (Invitrogen) for 12 min at 37°C in 5% CO₂. 2.5 × 10⁴ OVA-pulsed CD11b⁺ splenic cells were incubated with 20 × 10⁴ CFSE-labeled CD4 T cells in the presence or absence of 5 µg/ml CpG-B (ODN 1668) in a 96-well flat-bottom plate for 3 d at 37°C in 5% CO₂. All cultures were set up in triplicate. To harvest the cells, 7.5 mM EDTA was added to the cells for 15 min. Cells were then washed with MACS buffer and stained with anti-CD4 (BD Biosciences). A constant number of Calibrite APC beads (BD Biosciences) was added to allow the acquisition of equal parts per culture. 0.25 mg 7-aminoactinomycin D per test (BD Biosciences) was used to exclude the dead cells. For data acquisition, a constant number of Calibrite APC beads was counted. Live CD4 T cells (CD4⁺ 7-aminoactinomycin D⁻) were gated. The number of dividing cells (i.e., those showing less than the maximal CFSE fluorescence intensity) was determined as previously described (Cuda et al., 2015).

Isolation and adoptive transfer of lymphocytes

Isolation of single-cell suspension from the spleens of 8-wk-old B6.CD45.1 mice was performed as previously described (Rose et al., 2012). Splenic lymphocytes were purified by negative immune-magnetic selection. In brief, spleen cells were treated with Fc Block and incubated with PE-conjugated myeloid-lineage antibodies including anti-Ter119 (clone TER119; eBioscience), anti-CD11b (clone M1/70; BD Biosciences), anti-F4/80 (clone BM8; BioLegend), anti-CD11c (clone HL3; BD Biosciences), anti-mPDCA-1 (clone JF05-1C2.4.1; Miltenyi Biotec), anti-SiglecF (clone E50-2440; BD Biosciences), anti-NK1.1 (clone PK136; BD Biosciences), and anti-Ly6G (clone 1A8; BD Biosciences) followed by incubation of anti-PE MicroBeads (Miltenyi Biotec) and depletion on autoMACS Pro Separator (Miltenyi Biotec) with the “depletes” program. The resulting lymphocyte preparation was >80% purity as determined by flow cytometry. Each CD45.2. Rag^{-/-} or CD45.2. Rag^{-/-}LysM^{Cre}Bim^{fl/fl} mouse received ~4.0 × 10⁷ to 5.0 × 10⁷ donor lymphocytes through retro-orbital injections every month over an 8-mo period and bled every month to ensure the efficacy of adoptive transfer. The recipient CD45.2. Rag^{-/-} and CD45.2. Rag^{-/-}LysM^{Cre}Bim^{fl/fl} mice were then sacrificed after 8 mo of adoptive transfer to assess SLE-like disease symptoms.

Mixed bone marrow chimeras

Bone marrow was isolated from the femurs and tibias from 6-wk-old healthy donors from CTRL (Bim^{fl/fl}) and LysM^{Cre}

Bim^{fl/fl} mice. Red blood cells were lysed with Pharm Lyse Buffer (BD Biosciences). Enrichment of LSK (Lin⁻Sac-1⁺c-kit⁺) cells was performed via labeling cells with CD117 (c-kit) MicroBeads (Miltenyi Biotec) and positively selecting the c-kit⁺ cells on an autoMACS Pro Separator. The positively selected fraction was then incubated with Fc Block and labeled with fluorochrome-conjugated antibodies. LSK cells were obtained by FACS using a BD FACSARIA SORP instrument (BD Biosciences) at the Northwestern University Robert H. Lurie Comprehensive Cancer Center Flow Cytometry Core Facility. 3-mo-old recipient B6.CD45.1/.2 mice were subjected to a single dose of 1,000 cGy g-irradiation using a Cs-137-based Gammacell 40 irradiator (Best Theratronics). 12 h after irradiation, recipients were injected 2 × 10⁵ LSK cells from CTRL mice, 2 × 10⁵ LSK cells from LysM^{Cre}Bim^{fl/fl} or 10⁵ of LSK cells from each of CTRL and LysM^{Cre}Bim^{fl/fl} mice intravenously. Chimeric mice were given trimethoprim/sulfamethoxazole (40 mg/5 mg, respectively; Hi-Tech Pharmacal/Akorn) through autoclaved drinking water for 1 mo and then switched back to normal drinking water. Chimeras were assessed for SLE-like disease symptoms after 8 mo.

EdU study

CTRL (Bim^{fl/fl}) and LysM^{Cre}Bim^{fl/fl} mice were given 2 mg EdU (Santa Cruz Biotechnology, Inc.) through subcutaneous injections daily for 49 d. To examine turnover rate and proliferation in tissue-resident monocytes/macrophages, mice were sacrificed at several time points (days 35, 49, and 63). Single-cell suspensions from bone marrow, blood, spleen, and kidney were stained with fluorochrome-conjugated antibodies. EdU staining was assayed with intracellular flow cytometry using a Click-iT Plus EdU Alexa Fluor647 Flow Cytometry Assay kit (Invitrogen) according to the manufacturer's protocol. Each tissue came along with an FMO control to identify the EdU-positive cells. Stained cells were acquired on an LSRII flow cytometer. Compensation and data were analyzed using FlowJo software (Tree Star).

TUNEL analysis

Frozen spleen and kidney sections were cut at 4 µm thickness and fixed with 1% paraformaldehyde in PBS, pH 7.4, for 10 min at room temperature. Mouse thymus was used as a positive control for TUNEL. Slides were then postfixed in precooled ethanol/acetate 2:1 for 5 min at -20°C. TdT enzyme and dUTP-conjugated fluorescein cocktail were added according to manufacturer's protocol (ApopTag Peroxidase In Situ Apoptosis Detection kit; Millipore). Slides were mounted with mounting medium containing DAPI nuclei staining.

In vitro assays: Cell culture, cytokine measurements, and Western blot analysis

Bone marrow was prepared from the femurs and tibias, and erythrocytes were lysed. Bone marrow was then cultured in DMEM (Mediatech Inc.) supplemented with 10% heat-inactivated fetal bovine serum (ATLAS Biologicals), 2 mM L-glu-

tamine (Mediatech Inc.), 100 IU/ml penicillin, 100 μ g/ml streptomycin (Mediatech Inc.), and 1 mM sodium pyruvate (Mediatech Inc.) in the presence of 25 ng/ml recombinant murine GM-CSF (PeproTech, Inc.) or M-CSF (PeproTech, Inc.) at 37°C in 5% CO₂. Culture medium was changed on day 3 and day 5. (G)M-CSF BMDMs were seeded on day 7 at a concentration of 1.0–1.8 $\times 10^6$ cells/ml in the 6-well plates or 12 \times 75 mm culture tubes. For the cell death assay, growth factors were removed or kept in M-CSF BMDMs for 96 h at 37°C in 5% CO₂ and stained with Annexin V and Aqua Live/Dead. To measure cytokine fluctuations in response to TLR agonists, GM-CSF BMDMs were stimulated with or without 5 μ g/ml imiquimod (InvivoGen) or 5 μ g/ml CpG (InvivoGen) for 6 h, and supernatants were harvested for cytokine measurements using ProcartaPlex Multiplex Immunoassay kit (Affymetrix). For Western blot analysis, GM-CSF BMDMs were seeded at 3.2 $\times 10^5$ cells per well in a 24-well plate for 24 h before treatment. For poly(I:C) stimulation, GM-CSF BMDMs were mock transfected for 1 h or transfected with 0.5 μ g LMW-poly(I:C) (InvivoGen) per well at a final concentration of 1 μ g/ml for 1 or 2 h using 2.5 μ l Lipofectamine 2000 Reagent per 1 μ g poly(I:C). For LPS stimulation, GM-CSF BMDMs were treated with crude LPS (Sigma-Aldrich) at a final concentration of 100 ng/ml for 1 h. GM-CSF BMDMs were harvested in 150 μ l Laemmli, and 30 μ l of the protein lysate was separated by SDS-PAGE followed by immunoblot with phospho-TBK1, TBK1, phospho-IRF3 Bim or GAPDH (Cell Signaling Technology) at a dilution of 1:1,000. HRP-conjugated anti-rabbit IgG secondary antibody (GE Healthcare) was used at 1:6,000.

RNA-seq

Cells were sorted as described in “Tissue Preparation and Flow Cytometry” and immediately lysed with RLT Buffer from the Qiagen RNeasy Plus Mini kit or RNA extraction buffer from PicoPure RNA isolation kit (Arcturus Bioscience, Inc.). Cell lysates were stored at –80°C until RNA was extracted. RNA isolations were performed using the Qiagen RNeasy Plus Mini kit or PicoPure RNA isolation kit. RNA quality and quantity were measured using the Agilent Technologies High Sensitivity RNA ScreenTape System. SMA RT-Seq v4 Ultra Low Input RNA kit (Clontech Laboratories, Inc.) was used for full-length cDNA synthesis, and the Nextera XT DNA sample preparation kit (Illumina Inc.) was used for library preparation. DNA libraries were sequenced on an Illumina NextSeq 500 instrument with a target read depth of ~10 million aligned reads per sample. The pool was denatured and diluted, resulting in a 2.5 pM DNA solution. PhiX control was spiked at 1%, and the pool was sequenced by 1 \times 75 cycles using the NextSeq 500 High Output reagent kit (Illumina Inc.).

RNA-seq analysis

RNA-seq data were first demultiplexed using Bcl2fastq, and RNA-seq reads were aligned to the mouse reference genome

(NCBI, mm10) using TopHat and Bowtie aligners. Normalized gene counts were calculated using HT-seq. For the RNA-seq analysis, we focused on the set of highly expressed genes (log₂ normalized expression >4). For visualization, GENE-E (<https://software.broadinstitute.org/GENE-E/>) was used to generate pairwise correlation matrix (Pearson’s correlation) and to perform K-means clustering shown in the heat map. Volcano plots were generated using the log₂ fold change of normalized gene counts between control and LysM^{Cre}Bim^{fl/fl} cell populations (CD11b^{+/–}MZMs or kidney macrophages) on the x axis and p-values (–log₁₀) on the y axis. p-values were calculated with a two-tailed unpaired *t* test. The fold change scatterplots in Fig. 8 were constructed using log₂ fold change of normalized gene counts in control and LysM^{Cre}Bim^{fl/fl} kidney macrophages versus LysM^{Cre}Bim^{fl/fl} and TRIF^{–/–}LysM^{Cre}Bim^{fl/fl} kidney macrophages. Additional fold change scatterplots were generated in a similar fashion with NZB/W and LN patient data. GO associations and the related p-values were determined by GOrilla (Eden et al., 2009). Lists of differential genes, as in the Venn diagrams, were defined by log₂ fold change >1 and P < 0.01. The significance of the enrichment for overlapping genes in the Venn diagram was calculated using a hypergeometric distribution.

Microarray data comparison

Normalized gene expression files for NZB/W kidney macrophages and human LN were obtained through the Gene Expression Omnibus under accession numbers GSE32583 and GSE32591. The mouse genes were converted to the corresponding human orthologues using NCBI homologue (Build 68). The fold-change scatterplots in Fig. 9 (B–D) were constructed as described (see previous paragraph). Differential genes were defined using log₂ fold change >1 and P < 0.01, and Venn diagrams were used to compare the differential genes from RNA-seq analysis.

Statistical analysis

The data are presented as mean \pm SEM or mean \pm SD, and differences between groups were compared using the Mann–Whitney test or Student’s *t* test with GraphPad Prism 6.0 software.

Online supplemental material

Fig. S1 (related to Fig. 2) shows genomic confirmation of LysM^{Cre}Bim^{fl/fl} mice; LysM^{Cre}Bim^{fl/fl} mice are 98% on a C57BL/6J background, and the lack of Bim does not affect the balance between total expression levels of proapoptotic Bcl-2 members and antiapoptotic Bcl-2 members. Fig. S2 (related to Fig. 3) shows the alteration of the location of MZB cells in the spleen of LysM^{Cre}Bim^{fl/fl} mice. Fig. S3 (related to Fig. 5) shows that the deletion of Bim in lymphocytes is not sufficient to cause SLE-like disease. Fig. S4 (related to Fig. 6) shows Bim-BH3 has an antiinflammatory function. Fig. S5 (related to Fig. 7) shows that Bim-deleted BMDMs are more responsive to TLR agonists. Table S1 (related to Fig. S1 A) lists 150 SNP markers that are tested in the genomic

scan for $\text{LysM}^{\text{Cre}}\text{Bim}^{\text{fl/fl}}$ mice. Table S2 (related to Fig. 9 A) lists the overlapping genes shared by $\text{LysM}^{\text{Cre}}\text{Bim}^{\text{fl/fl}}$ kidney macrophages, $\text{CD11b}^+\text{MZMs}$, and $\text{CD11b}^-\text{MZMs}$. Table S3 (related to Fig. 9, E and F) lists the overlapping genes shared by $\text{LysM}^{\text{Cre}}\text{Bim}^{\text{fl/fl}}$ kidney macrophages and NZB/W kidney macrophages and $\text{LysM}^{\text{Cre}}\text{Bim}^{\text{fl/fl}}$ kidney macrophages and kidney tissue of LN patients.

ACKNOWLEDGMENTS

We thank the members of the Perlman Laboratory for helpful comments. We also thank David A. Hildeman (Department of Immunobiology, Cincinnati Children's Hospital at the University of Cincinnati College of Medicine) for his gift of the $\text{CD4}^{\text{Cre}}\text{Bim}^{\text{fl/fl}}$ and $\text{dLck}^{\text{Cre}}\text{Bim}^{\text{fl/fl}}$ mice.

The research was supported by the American Heart Association (grant PRE21410010 to F. Tsai), the National Institutes of Health (grant K01AR064313 to C.M. Cuda and grants HL108795, AR050250, AR054796, AR064546, and AI092490 to H. Perlman), the United States-Israel Binational Science Foundation (grant 2013247), the Rheumatology Research Foundation (grant Agmt 05/06/14), and the Mabel Green Myers Chair of Medicine (H. Perlman). Flow Cytometry Cell Sorting was performed on a BD FACSAria SORP system, which was purchased through the support of the National Institutes of Health (grant 1S100D011996-01). Flow cytometry and histology services were provided by the Northwestern University Lurie Cancer Flow Cytometry facility and Mouse Histology and Phenotyping Laboratory, which are supported by the National Cancer Institute (grant P30-CA060553 awarded to the Robert H Lurie Comprehensive Cancer Center).

The authors declare no competing financial interests.

Author contributions: Conceptualization, F. Tsai, C.M. Cuda, and H. Perlman; Methodology, F. Tsai, P.J. Homan, A.V. Misharin, P. Bouillet, C.M. Cuda, and H. Perlman; Formal analysis, F. Tsai, P.J. Homan, D.R. Winter, and C.M. Cuda; Investigation, F. Tsai, P.J. Homan, H. Abdala-Valencia, A.V. Misharin, H. Abdala-Valencia, G.K. Haines III, S. Dominguez, R. Saber, A. Chang, C. Mohan, J. Hutcheson, A. Davidson, G.R.S. Budinger, P. Bouillet, A. Dorfleutner, C. Stehlik, D.R. Winter, C.M. Cuda, and H. Perlman; Resources, C. Mohan, P. Bouillet, and H. Perlman; Writing—Original Draft, F. Tsai, C.M. Cuda, and H. Perlman; Writing—Review & Editing, F. Tsai, G.R.S. Budinger, D.R. Winter, C.M. Cuda, and H. Perlman; Visualization, F. Tsai; Supervision, C.M. Cuda and H. Perlman; Funding Acquisition, F. Tsai, C.M. Cuda, and H. Perlman.

Submitted: 14 March 2017

Revised: 25 July 2017

Accepted: 6 September 2017

REFERENCES

- Baccala, R., K. Hoebe, D.H. Kono, B. Beutler, and A.N. Theofilopoulos. 2007. TLR-dependent and TLR-independent pathways of type I interferon induction in systemic autoimmunity. *Nat. Med.* 13:543–551. <https://doi.org/10.1038/nm1590>
- Ban, T., G.R. Sato, A. Nishiyama, A. Akiyama, M. Takasuna, M. Umehara, S. Suzuki, M. Ichino, S. Matsunaga, A. Kimura, et al. 2016. Lyn Kinase Suppresses the Transcriptional Activity of IRF5 in the TLR-MyD88 Pathway to Restrain the Development of Autoimmunity. *Immunity* 45:319–332. <https://doi.org/10.1016/j.immuni.2016.07.015>
- Berthier, C.C., R. Bethunaickan, T. Gonzalez-Rivera, V. Nair, M. Ramanujam, W. Zhang, E.P. Bottinger, S. Segerer, M. Lindenmeyer, C.D. Cohen, et al. 2012. Cross-species transcriptional network analysis defines shared inflammatory responses in murine and human lupus nephritis. *J. Immunol.* 189:988–1001. <https://doi.org/10.4049/jimmunol.1103031>
- Billard, C. 2013. BH3 mimetics: status of the field and new developments. *Mol. Cancer Ther.* 12:1691–1700. <https://doi.org/10.1158/1535-7163.MCT-13-0058>
- Bouillet, P., D. Metcalf, D.C. Huang, D.M. Tarlinton, T.W. Kay, F. Köntgen, J.M. Adams, and A. Strasser. 1999. Proapoptotic Bcl-2 relative Bim required for certain apoptotic responses, leukocyte homeostasis, and to preclude autoimmunity. *Science*. 286:1735–1738. <https://doi.org/10.1126/science.286.5445.1735>
- Bouillet, P., J.F. Purton, D.I. Godfrey, L.C. Zhang, L. Coultas, H. Puthalakath, M. Pellegrini, S. Cory, J.M. Adams, and A. Strasser. 2002. BH3-only Bcl-2 family member Bim is required for apoptosis of autoreactive thymocytes. *Nature*. 415:922–926. <https://doi.org/10.1038/415922a>
- Chen, M., L. Huang, and J. Wang. 2007. Deficiency of Bim in dendritic cells contributes to over-activation of lymphocytes and autoimmunity. *Blood*. 109:4360–4367. <https://doi.org/10.1182/blood-2006-11-056424>
- Cuda, C.M., H. Agrawal, A.V. Misharin, G.K. Haines III, J. Hutcheson, E. Weber, J.A. Schoenfeldt, C. Mohan, R.M. Pope, and H. Perlman. 2012. Requirement of myeloid cell-specific Fas expression for prevention of systemic autoimmunity in mice. *Arthritis Rheum.* 64:808–820. <https://doi.org/10.1002/art.34317>
- Cuda, C.M., A.V. Misharin, A.K. Gierut, R. Saber, G.K. Haines III, J. Hutcheson, S.M. Hedrick, C. Mohan, G.S. Budinger, C. Stehlik, and H. Perlman. 2014. Caspase-8 acts as a molecular rheostat to limit RIPK1- and MyD88-mediated dendritic cell activation. *J. Immunol.* 192:5548–5560. <https://doi.org/10.4049/jimmunol.1400122>
- Cuda, C.M., A.V. Misharin, S. Khare, R. Saber, F. Tsai, A.M. Archer, P.J. Homan, G.K. Haines III, J. Hutcheson, A. Dorfleutner, et al. 2015. Conditional deletion of caspase-8 in macrophages alters macrophage activation in a RIPK-dependent manner. *Arthritis Res. Ther.* 17:291. <https://doi.org/10.1186/s13075-015-0794-z>
- Dai, S., R. Jia, X. Zhang, Q. Fang, and L. Huang. 2014. The PD-1/PD-Ls pathway and autoimmune diseases. *Cell. Immunol.* 290:72–79. <https://doi.org/10.1016/j.cellimm.2014.05.006>
- Eden, E., R. Navon, I. Steinfeld, D. Lipson, and Z. Yakhini. 2009. GOrrilla: a tool for discovery and visualization of enriched GO terms in ranked gene lists. *BMC Bioinformatics*. 10:48. <https://doi.org/10.1186/1471-2105-10-48>
- Feng, X., H. Wu, J.M. Grossman, P. Hanvivadhanakul, J.D. FitzGerald, G.S. Park, X. Dong, W. Chen, M.H. Kim, H.H. Weng, et al. 2006. Association of increased interferon-inducible gene expression with disease activity and lupus nephritis in patients with systemic lupus erythematosus. *Arthritis Rheum.* 54:2951–2962. <https://doi.org/10.1002/art.22044>
- Gautier, E.L., T. Huby, F. Saint-Charles, B. Ouzilleau, M.J. Chapman, and P. Lesnik. 2008. Enhanced dendritic cell survival attenuates lipopolysaccharide-induced immunosuppression and increases resistance to lethal endotoxic shock. *J. Immunol.* 180:6941–6946. <https://doi.org/10.4049/jimmunol.180.10.6941>
- Ge, Y., C. Jiang, S.S. Sung, H. Bagavant, C. Dai, H. Wang, C.C. Kannapell, H.P. Cathro, F. Gaskin, and S.M. Fu. 2013. Cgzn1 allele confers kidney resistance to damage preventing progression of immune complex-mediated acute lupus glomerulonephritis. *J. Exp. Med.* 210:2387–2401. <https://doi.org/10.1084/jem.20130731>
- Ginhoux, F., and S. Jung. 2014. Monocytes and macrophages: developmental pathways and tissue homeostasis. *Nat. Rev. Immunol.* 14:392–404. <https://doi.org/10.1038/nri3671>
- Herold, M.J., R. Stuchbery, D. Mérino, T. Willson, A. Strasser, D. Hildeman, and P. Bouillet. 2014. Impact of conditional deletion of the pro-apoptotic BCL-2 family member BIM in mice. *Cell Death Dis.* 5:e1446. <https://doi.org/10.1038/cddis.2014.409>
- Hill, G.S., M. Delahousse, D. Nochy, E. Tomkiewicz, P. Rémy, F. Mignon, and J.P. Méry. 2000. A new morphologic index for the evaluation of renal biopsies in lupus nephritis. *Kidney Int.* 58:1160–1173. <https://doi.org/10.1046/j.1523-1755.2000.00272.x>
- Hill, G.S., M. Delahousse, D. Nochy, P. Rémy, F. Mignon, J.P. Méry, and J. Bariéty. 2001. Predictive power of the second renal biopsy in lupus nephritis: significance of macrophages. *Kidney Int.* 59:304–316. <https://doi.org/10.1046/j.1523-1755.2001.00492.x>

- Hou, W.S., and L. Van Parijs. 2004. A Bcl-2-dependent molecular timer regulates the lifespan and immunogenicity of dendritic cells. *Nat. Immunol.* 5:583–589. <https://doi.org/10.1038/ni1071>
- Hutcheson, J., and H. Perlman. 2008. BH3-only proteins in rheumatoid arthritis: potential targets for therapeutic intervention. *Oncogene.* 27(Suppl 1):S168–S175. <https://doi.org/10.1038/onc.2009.54>
- Hutcheson, J., J.C. Scatizzi, A.M. Siddiqui, G.K. Haines III, T. Wu, Q.Z. Li, L.S. Davis, C. Mohan, and H. Perlman. 2008. Combined deficiency of proapoptotic regulators Bim and Fas results in the early onset of systemic autoimmunity. *Immunity.* 28:206–217. <https://doi.org/10.1016/j.immuni.2007.12.015>
- Katsiari, C.G., S.N. Lioussis, and P.P. Sfikakis. 2010. The pathophysiologic role of monocytes and macrophages in systemic lupus erythematosus: a reappraisal. *Semin. Arthritis Rheum.* 39:491–503. <https://doi.org/10.1016/j.semarthrit.2008.11.002>
- Kim, W.U., A. Sreih, and R. Bucala. 2009. Toll-like receptors in systemic lupus erythematosus: prospects for therapeutic intervention. *Autoimmun. Rev.* 8:204–208. <https://doi.org/10.1016/j.autrev.2008.07.046>
- Li, H., Y.X. Fu, Q. Wu, Y. Zhou, D.K. Crossman, P. Yang, J. Li, B. Luo, L.M. Morel, J.H. Kabarowski, et al. 2015. Interferon-induced mechanosensing defects impede apoptotic cell clearance in lupus. *J. Clin. Invest.* 125:2877–2890. <https://doi.org/10.1172/JCI81059>
- Li, K.P., A. Fährlich, E. Roy, C.M. Cuda, H.L. Grimes, H.R. Perlman, K. Kalies, and D.A. Hildeman. 2017. Temporal Expression of Bim Limits the Development of Agonist-Selected Thymocytes and Skews Their TCR β Repertoire. *J. Immunol.* 198:257–269. <https://doi.org/10.1094/jimmunol.1601200>
- Mason, K.D., A. Lin, L. Robb, E.C. Josefsson, K.J. Henley, D.H. Gray, B.T. Kile, A.W. Roberts, A. Strasser, D.C. Huang, et al. 2013. Proapoptotic Bak and Bax guard against fatal systemic and organ-specific autoimmune disease. *Proc. Natl. Acad. Sci. USA.* 110:2599–2604. <https://doi.org/10.1073/pnas.1215097110>
- McGaha, T.L., and M.C. Karlsson. 2016. Apoptotic cell responses in the splenic marginal zone: a paradigm for immunologic reactions to apoptotic antigens with implications for autoimmunity. *Immunol. Rev.* 269:26–43. <https://doi.org/10.1111/imr.12382>
- Mérino, D., M. Giam, P.D. Hughes, O.M. Siggs, K. Heger, L.A. O'Reilly, J.M. Adams, A. Strasser, E.F. Lee, W.D. Fairlie, and P. Bouillet. 2009. The role of BH3-only protein Bim extends beyond inhibiting Bcl-2-like prosurvival proteins. *J. Cell Biol.* 186:355–362. <https://doi.org/10.1083/jcb.200905153>
- Miyamoto, T., H. Iwasaki, B. Reizis, M. Ye, T. Graf, I.L. Weissman, and K. Akashi. 2002. Myeloid or lymphoid promiscuity as a critical step in hematopoietic lineage commitment. *Dev. Cell.* 3:137–147. [https://doi.org/10.1016/S1534-5807\(02\)00201-0](https://doi.org/10.1016/S1534-5807(02)00201-0)
- Nickerson, K.M., S.R. Christensen, J. Shupe, M. Kashgarian, D. Kim, K. Elkon, and M.J. Shlomchik. 2010. TLR9 regulates TLR7- and MyD88-dependent autoantibody production and disease in a murine model of lupus. *J. Immunol.* 184:1840–1848. <https://doi.org/10.4049/jimmunol.0902592>
- Nopora, A., and T. Brocker. 2002. Bcl-2 controls dendritic cell longevity in vivo. *J. Immunol.* 169:3006–3014. <https://doi.org/10.4049/jimmunol.169.6.3006>
- Obata, Y., T. Tanaka, E. Stockert, and R.A. Good. 1979. Autoimmune and lymphoproliferative disease in (B6-GIX+ X 129)F1 mice: relation to naturally occurring antibodies against murine leukemia virus-related cell surface antigens. *Proc. Natl. Acad. Sci. USA.* 76:5289–5293. <https://doi.org/10.1073/pnas.76.10.5289>
- Rai, R., S.K. Chauhan, V.V. Singh, M. Rai, and G. Rai. 2016. RNA-seq Analysis Reveals Unique Transcriptome Signatures in Systemic Lupus Erythematosus Patients with Distinct Autoantibody Specificities. *PLoS One.* 11:e0166312. <https://doi.org/10.1371/journal.pone.0166312>
- Rose, S., A. Misharin, and H. Perlman. 2012. A novel Ly6C/Ly6G-based strategy to analyze the mouse splenic myeloid compartment. *Cytometry A.* 81:343–350. <https://doi.org/10.1002/cyto.a.22012>
- Scatizzi, J.C., J. Hutcheson, R.M. Pope, G.S. Firestein, A.E. Koch, M. Mavers, A. Smason, H. Agrawal, G.K. Haines III, N.S. Chandel, et al. 2010. Bim-Bcl-2 homology 3 mimetic therapy is effective at suppressing inflammatory arthritis through the activation of myeloid cell apoptosis. *Arthritis Rheum.* 62:441–451. <https://doi.org/10.1002/art.27198>
- Shirai, T., and S. Hirose. 2006. Molecular pathogenesis of SLE. *Springer Semin. Immunopathol.* 28:79–82. <https://doi.org/10.1007/s00281-006-0032-5>
- Steimer, D.A., K. Boyd, O. Takeuchi, J.K. Fisher, G.P. Zambetti, and J.T. Opferman. 2009. Selective roles for antiapoptotic MCL-1 during granulocyte development and macrophage effector function. *Blood.* 113:2805–2815. <https://doi.org/10.1182/blood-2008-05-159145>
- Takeuchi, O., J. Fisher, H. Suh, H. Harada, B.A. Malynn, and S.J. Korsmeyer. 2005. Essential role of BAX, BAK in B cell homeostasis and prevention of autoimmune disease. *Proc. Natl. Acad. Sci. USA.* 102:11272–11277. <https://doi.org/10.1073/pnas.0504783102>
- Teichmann, L.L., M.L. Ols, M. Kashgarian, B. Reizis, D.H. Kaplan, and M.J. Shlomchik. 2010. Dendritic cells in lupus are not required for activation of T and B cells but promote their expansion, resulting in tissue damage. *Immunity.* 33:967–978. <https://doi.org/10.1016/j.immuni.2010.11.025>
- Tesch, G.H., S. Maifert, A. Schwarting, B.J. Rollins, and V.R. Kelley. 1999. Monocyte chemoattractant protein 1-dependent leukocytic infiltrates are responsible for autoimmune disease in MRL-Fas(lpr) mice. *J. Exp. Med.* 190:1813–1824. <https://doi.org/10.1084/jem.190.12.1813>
- Tsokos, G.C., M.S. Lo, P. Costa Reis, and K.E. Sullivan. 2016. New insights into the immunopathogenesis of systemic lupus erythematosus. *Nat. Rev. Rheumatol.* 12:716–730. <https://doi.org/10.1038/nrrheum.2016.186>
- Ye, M., H. Iwasaki, C.V. Laiosa, M. Stadtfeld, H. Xie, S. Heck, B. Clausen, K. Akashi, and T. Graf. 2003. Hematopoietic stem cells expressing the myeloid lysozyme gene retain long-term, multilineage repopulation potential. *Immunity.* 19:689–699. [https://doi.org/10.1016/S1074-7613\(03\)00299-1](https://doi.org/10.1016/S1074-7613(03)00299-1)
- Yeretssian, G., R.G. Correa, K. Doiron, P. Fitzgerald, C.P. Dillon, D.R. Green, J.C. Reed, and M. Saleh. 2011. Non-apoptotic role of BID in inflammation and innate immunity. *Nature.* 474:96–99. <https://doi.org/10.1038/nature09982>

SUPPLEMENTAL MATERIAL

Tsai et al., <https://doi.org/10.1084/jem.20170479>

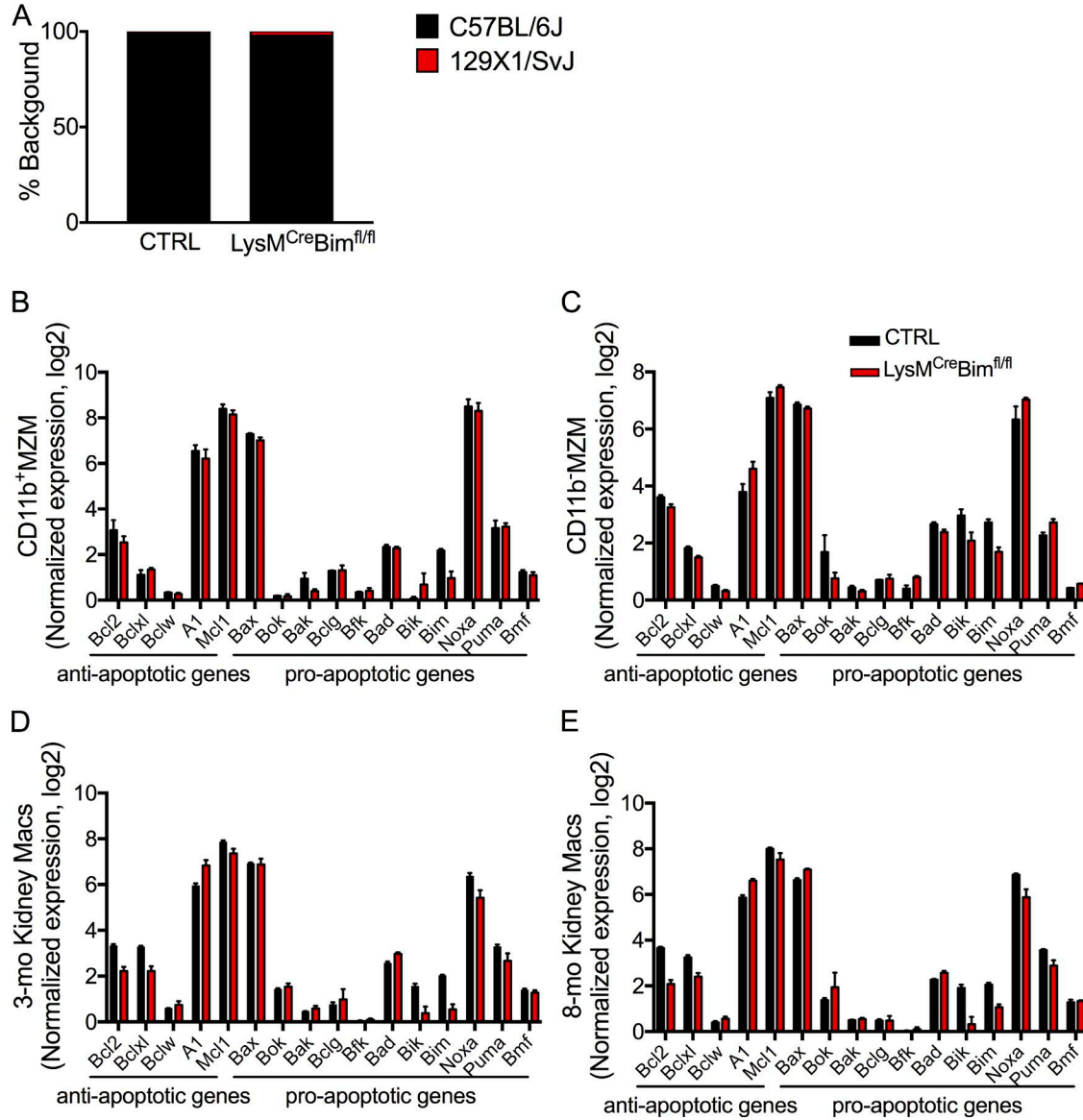


Figure S1. **Genomic confirmation of LysM^{Cre}Bim^{fl/fl} mice.** (A) LysM^{Cre}Bim^{fl/fl} mice are 98% on a C57BL/6J background (black bar) and only 2% on a 129X1/SvJ background (red bar) as demonstrated by SNP genomic screening. (B–E) Gene expression of the Bcl-2 family members, including five prosurvival members and all proapoptotic members in splenic CD11b⁺ MZMs (B), splenic CD11b⁻ MZMs (C), 3-mo-old kidney macrophages (D), and 8-mo-old kidney macrophages (E; CTRL, $n \geq 2$; LysM^{Cre}Bim^{fl/fl}, $n \geq 2$). Data are represented as mean \pm SEMs and compared by Mann–Whitney test.

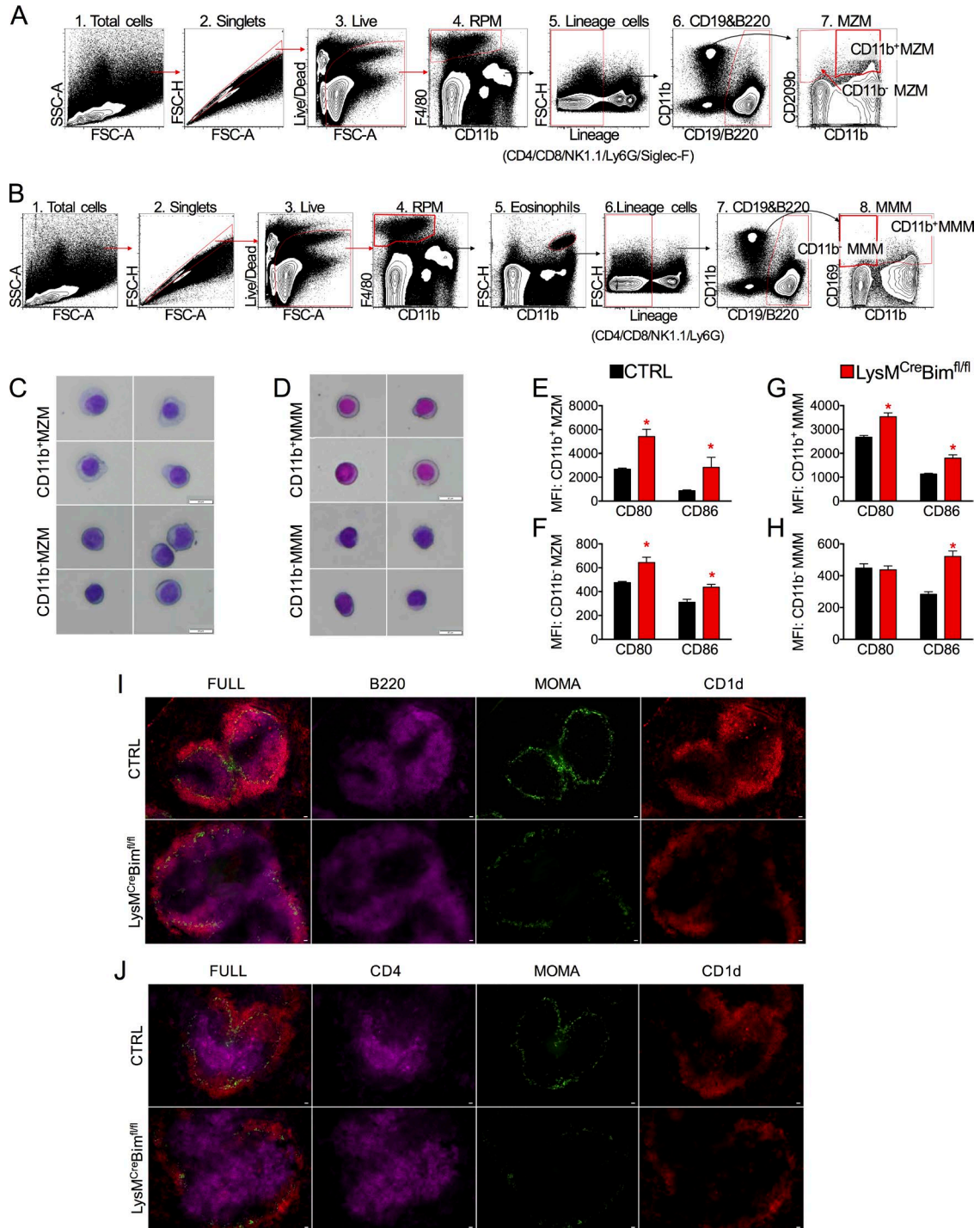


Figure S2. **Alteration of MZMs and MZB cells in the spleen of *LysM^{Cre}Bim^{fl/fl}* mice.** (A–H) MZMs from 8-mo-old female *LysM^{Cre}Bim^{fl/fl}* mice ($n = 5$) exhibited heightened activity. Flow gating strategy used to identify MZMs (A) and MMMs (B). Representative photomicrographs of sorted CD11b⁺MZMs and CD11b⁻ MZMs (C) and CD11b⁺ MMMs and CD11b⁻ MMMs (D). Bars, 20 μ m. Expression of CD80 and CD86 were evaluated on CD11b⁺ MZMs (E), CD11b⁻ MZMs (F), CD11b⁺ MMMs (G), and CD11b⁻ MMMs (H). (I and J) Disappearance of MZB cells in the spleen of *LysM^{Cre}Bim^{fl/fl}* mice. (I) Representative photomicrographs of spleen frozen sections stained with B220-APC (purple), MOMA(CD169)-FITC (green), and CD1d-PE (red). MZB cells are stained CD1d⁺ (bright pink). Bars, 20 μ m. (J) Representative photomicrographs of 8- μ m frozen spleen sections stained with CD4-APC (purple), MOMA(CD169)-FITC (green), and CD1d-PE (red). MZB cells are stained CD1d⁺ (red). Bars, 20 μ m. Representative data from two independent experiments are presented as mean \pm SEMs and were compared by Mann–Whitney test. Asterisk indicates a significant difference between *LysM^{Cre}Bim^{fl/fl}* and CTRL (*, $P < 0.05$). MFI, mean fluorescence intensity; RPM, red-pulp macrophage.

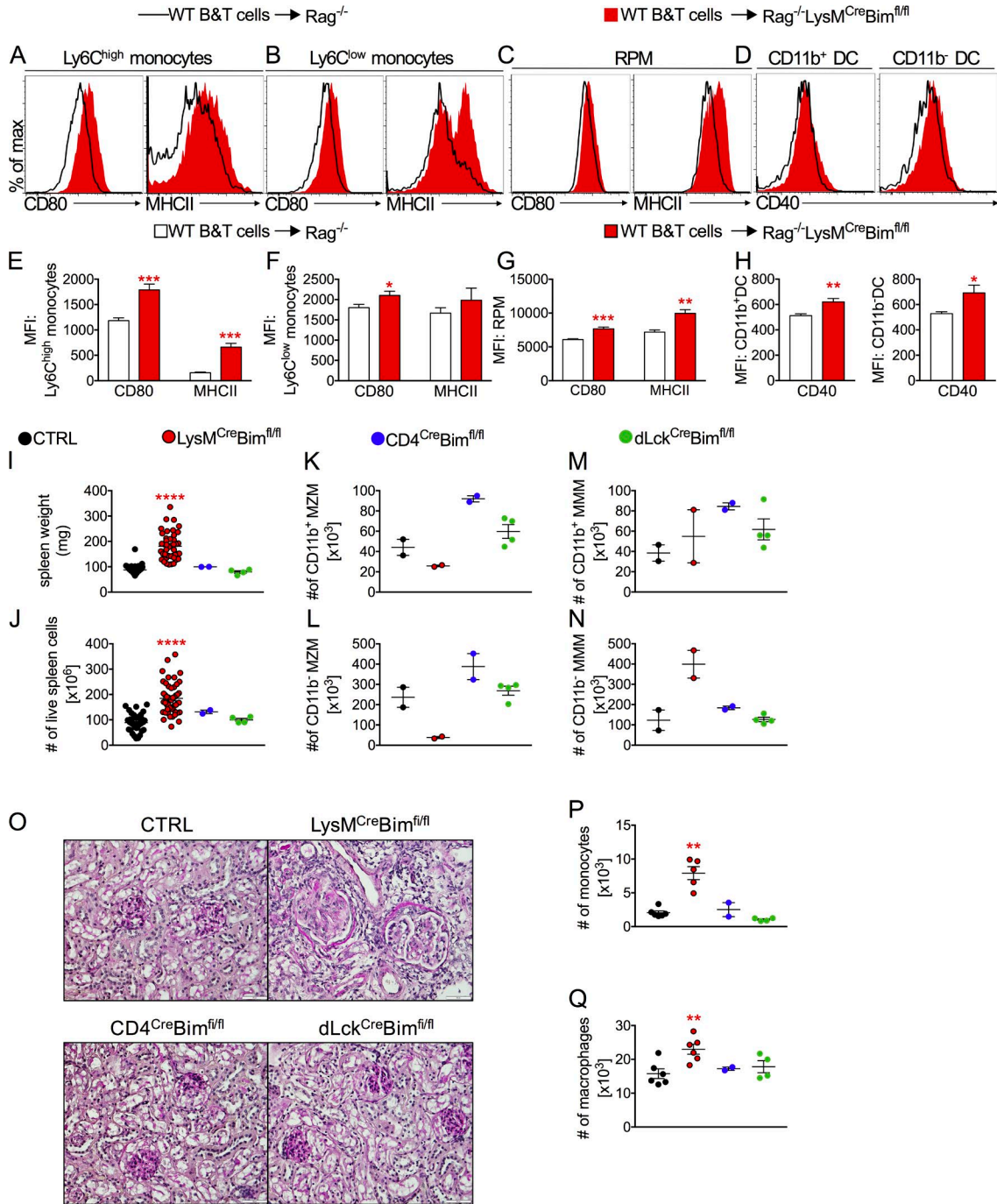


Figure S3. Bim-deleted myeloid cells are the drivers of systemic autoimmunity. (A–H) Quantitative analysis of expression of CD80 and MHCII or CD40 on Ly6C^{high} monocytes (A and E), Ly6C^{low} monocytes (B and F), red-pulp macrophages (RPM; C and G), and CD11b⁺ and CD11b⁻ DCs (D and H). Representative data from two independent experiments are shown (WT B and T cells → Rag^{-/-} mice, $n \geq 7$, WT B and T cells → Rag^{-/-}LysM^{Cre}Bim^{fl/fl}, $n \geq 8$). Data are presented as mean \pm SEMs and were compared by Mann–Whitney test. Asterisks indicate a significant difference between WT B and T cells → Rag^{-/-}LysM^{Cre}Bim^{fl/fl} and WT B and T cells → Rag^{-/-} mice (*, $P < 0.05$; **, $P < 0.01$; ***, $P < 0.001$). (I–Q) 8-mo-old female CTRL (C57BL/6, $n \geq 2$), LysM^{Cre}Bim^{fl/fl} (C57BL/6, $n \geq 2$), CD4^{Cre}Bim^{fl/fl} (C57BL/6, $n = 2$), and dLck^{Cre}Bim^{fl/fl} (C57BL/6, $n = 6$) mice were examined for systemic autoimmune disease phenotypes. (I) Spleen weights. (J) Total number of live spleen cells. Quantitative analysis of splenic MZM and MMM showing the number of CD11b⁺ MZMs (K), CD11b⁻ MZMs (L), CD11b⁺ MMMs (M), and CD11b⁻ MMMs (N). (O) Representative photomicrographs of PAS-stained kidney sections. Bars, 50 μ m. (P and Q) Flow cytometric analysis for numbers of infiltrating kidney monocytes (P) and infiltrating kidney macrophages (Q). The experiment was performed one time. Data are presented as mean \pm SEM and were compared by Mann–Whitney test. Asterisks indicate a significant difference between LysM^{Cre}Bim^{fl/fl} and CTRL (**, $P < 0.01$; ***, $P < 0.0001$). MFI, mean fluorescence intensity.

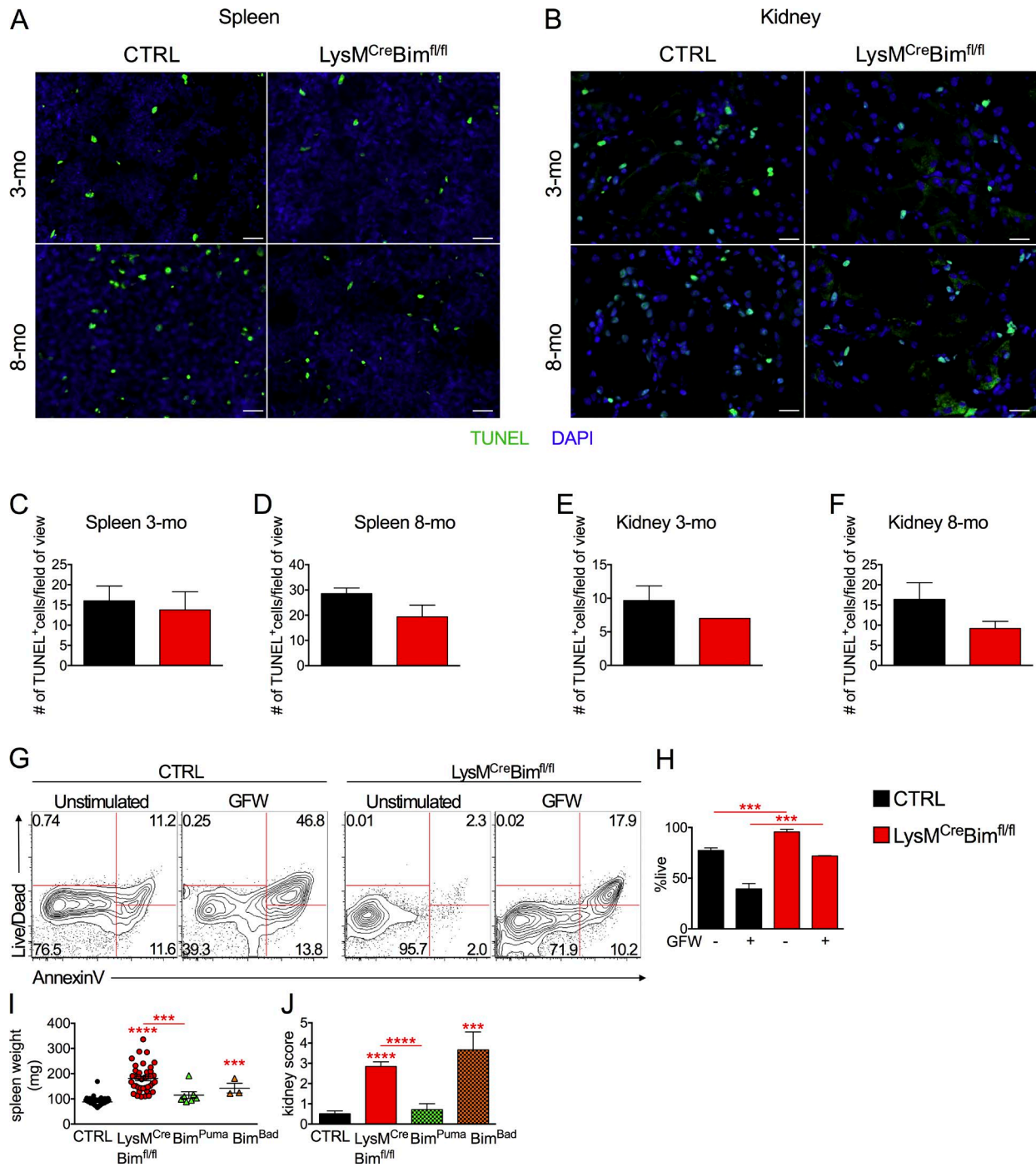


Figure S4. **Bim** may have a nonapoptotic function in myeloid cells. (A–F) TUNEL assay in spleen and kidney from 3- and 8-mo-old CTRL ($n = 3$) and LysM^{Cre}Bim^{fl/fl} ($n = 3$) mice. (A and B) Representative photomicrographs for apoptotic cells in spleen (A) and kidney (B). TUNEL-FITC (green), DAPI (blue). Bars, 20 μ m. (C–F) Number of TUNEL⁺ cells per field of view in 3-mo-old (C) and 8-mo-old spleens (D) and 3-mo-old (E) and 8-mo-old kidney (F). Representative data from three independent experiments are presented as mean \pm SEM and were compared by Mann–Whitney test. (G and H) Loss of Bim in BMDMs enhanced survival. BMDMs CTRL ($n = 3$) and LysM^{Cre}Bim^{fl/fl} ($n = 3$) were deprived of growth factors (GFW) for 96 h and then stained with Annexin V and Live/Dead. Data represent the percentage of live cells. Representative data from three independent experiments are presented as mean \pm SD and were compared by Student’s t test. Asterisk indicates a significant difference between LysM^{Cre}Bim^{fl/fl} and CTRL (***, $P < 0.001$). (I) Spleen weights for 6-mo-old CTRL ($n = 46$), LysM^{Cre}Bim^{fl/fl} ($n = 39$), Bim^{Puma} ($n = 7$), and Bim^{Bad} ($n = 3$) mice. (J) Kidney sections scored for kidney damage. Data were obtained from indicated number of mice in three experiments. Asterisk indicates a significant difference between LysM^{Cre}Bim^{fl/fl} or Bim^{Bad} and CTRL (***, $P < 0.001$; ****, $P < 0.0001$).

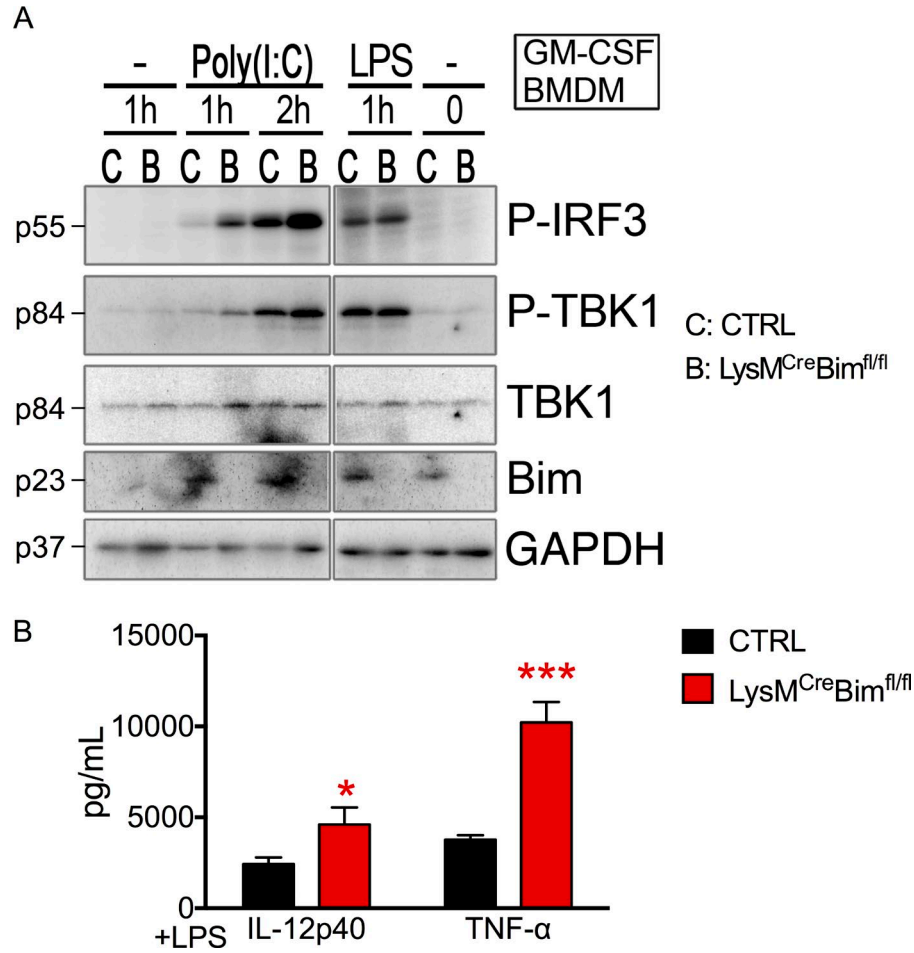


Figure S5. **Bim-deleted BMDMs are more responsive to TLR agonists.** (A) Loss of Bim in BMDMs up-regulates the TLR3-TBK1-IRF3 pathway, as treatment with the TLR3 agonist poly(I:C) induced more p-IRF3 and p-TBK1 expression in $LysM^{Cre}Bim^{fl/fl}$ BMDMs. (B) BMDMs were stimulated with LPS for 6 h, and supernatants were collected and evaluated for IL-12p40 and TNF by multiplex immunoassay as described in Materials and methods. Representative data from two independent experiments (CTRL, $n = 3$, $LysM^{Cre}Bim^{fl/fl}$, $n = 3$) are presented as mean \pm SD and were compared by Student's t test. Asterisks indicate a significant difference between $LysM^{Cre}Bim^{fl/fl}$ and CTRL (*, $P < 0.05$; ***, $P < 0.001$).

Table S1. SNP markers used in the genome scan

Chromosome location	RS number	C57BL/6J	129X1/SvJ	LysM ^{Cre} Bim ^{f/f}	
1	rs3708040	C	T	C	
	rs3666554	G	T	G	
	rs3654040	A	C	A	
	rs3022802	T	G	T	
	rs3678377	A	G	G/A	
	rs13476020	G	T	G/T	
	rs3676992	G	T	G	
	rs3663996	A	G	A	
	rs3706326	G	A	G	
	rs3714281	C	T	C	
	2	rs3713997	G	A	G
		rs4139548	A	G	A
		rs3697051	C	G	C
		rs3714030	T	C	T
rs3670874		T	G	T	
rs3686727		A	G	A	
rs3691456		A	T	A	
rs3726475		T	A	A	
rs3022939		T	C	T/C	
rs13476938		T	C	T	
3		rs3680834	G	C	G
		rs3709272	T	C	T
		rs3709395	C	T	C
		rs3659459	A	T	A
	rs13459185	C	T	C	
	rs3708141	A	G	A	
	rs3668158	G	A	G	
	rs3686542	T	C	T	
	4	rs3694594	G	T	G
		rs4138316	C	T	C
		rs3723778	C	G	C
		rs3654495	C	T	C
		rs4139273	G	A	G
		rs3704372	C	T	C
rs13477949		A	T	A	
rs3718220		A	G	A	
rs3680364		G	T	G	
5		rs4225033	G	A	G
		rs3664933	C	G	C
		rs3023833	A	C	A
		rs4225249	A	G	A
		rs3657487	A	G	A
	rs3656524	T	C	T	
	rs3705399	T	C	T	
	rs3705356	G	T	G	
	6	rs3661828	C	T	C
		rs13478656	C	T	C
		rs13478727	A	C	A
		rs3706318	A	G	A
		rs3707989	G	T	G
		rs3727110	T	A	T
rs13479079		C	G	C	
7		rs3655750	T	C	T
		rs13479217	A	G	A
		rs6267233	T	G	T
		rs3701187	T	C	T
		rs3674350	T	G	T
		rs3717698	C	T	C
		rs3664224	C	T	C
	8	rs3701395	T	C	T
		rs3691954	G	A	G
		rs3719876	T	A	T

Table S1. SNP markers used in the genome scan (Continued)

Chromosome location	RS number	C57BL/6J	129X1/SvJ	LysM ^{Cre} Bim ^{f/f}
	rs3661085	C	G	C
	rs3722665	G	T	G
	rs3089148	A	C	A
	rs3023718	G	A	G
	rs4227443	C	T	C
9	rs3694533	T	C	T
	rs13480104	G	C	G
	rs3653389	C	T	C
	rs4227706	T	C	T
	rs3687598	C	A	C
	rs3679358	T	C	T
	rs3706619	G	A	G
10	rs3090968	A	T	A
	rs3665690	A	G	A
	rs3716113	T	C	T
	rs13480619	T	C	T
	rs13480654	A	G	A
	rs3704566	T	C	T
	rs3713628	T	C	T
	rs3719409	G	A	G
11	rs3659787	G	A	G
	rs3673413	G	A	G
	rs3691185	A	G	A
	rs3024185	G	A	G
	rs3663879	G	C	G
	rs4229101	G	A	G
	rs3675603	C	T	C
12	rs3675632	G	T	G
	rs3023339	A	C	A
	rs3701242	G	A	G
	rs3657568	C	A	C
	rs3663221	A	G	A
	rs3719660	G	C	G
	rs3686631	A	T	A
13	rs3695486	A	G	A
	rs13481730	G	A	G
	rs3679151	A	T	A
	rs3654821	C	T	C
	rs13481910	C	G	C
13-100574867-N	SNP genomic scan performed by the Jackson Laboratory	T	A	T
14	rs3689508	T	A	T
	rs3719262	A	G	A
	rs3023408	T	G	T
	rs4230463	A	G	A
	rs4230463	G	A	G
	rs4230603	G	A	G
15	rs3687235	A	G	A
	rs13482478	C	T	C
	rs3667271	G	C	G
	rs4230758	C	T	C
	rs4230879	G	A	G
	rs3023831	T	C	T
16	rs4153115	G	T	G/T
	rs4165467	G	C	G
	rs4180179	G	A	A/G
	rs4195412	A	G	A
	rs4211695	G	C	G
	rs4221067	C	T	C

Table S1. SNP markers used in the genome scan (Continued)

Chromosome location	RS number	C57BL/6J	129X1/SvJ	LysM ^{Cre} Bim ^{f/f}
17	rs3667161	A	G	A
	rs4137889	G	A	G
	rs3677240	G	A	G
	rs13483064	T	C	T
	rs3707550	T	A	T
18	rs3706767	T	C	T
	rs3714233	T	C	T
	rs3715080	T	A	T
	rs3023828	C	T	C
	rs3663208	G	T	G
19	rs3726735	A	G	A
	rs3023517	A	G	A
M-05782_1	rs3023106	T	G	T
X	rs13483721	C	A	C
	rs13483729	C	G	C
	rs13483772	C	A	C
	rs3664154	C	T	C
	rs13483921	G	A	G
	rs3706437	G	T	G
	rs13484036	T	C	T

Table S2. List of genes shared among kidney macrophages, CD11b⁺ MZMs, and CD11b⁻ MZMs from LysM^{Cre}Bim^{f/f} mice

Kidney macrophages versus CD11b ⁻ MZM	Kidney macrophages versus CD11b ⁺ MZM	CD11b ⁻ MZM versus CD11b ⁺ MZM
<i>Lyz2</i> ^a	<i>Lyz2</i> ^a	<i>Lyz2</i> ^a
<i>Hjurp</i>	<i>Hjurp</i>	<i>Nudt17</i>
<i>Ms4a6d</i>		

^aOverlapping genes.

Table S3. List of genes shared among LysM^{Cre}Bim^{f/f} kidney macrophages, NZB/W kidney macrophages, and kidney tissue of lupus nephritis patients

LysM ^{Cre} Bim ^{f/f} kidney macrophages versus NZB/W kidney macrophages (n = 33)		LysM ^{Cre} Bim ^{f/f} kidney macrophages versus glomeruli tissue of human LN (n = 5)	LysM ^{Cre} Bim ^{f/f} kidney macrophages versus tubular tissue of human LN (n = 7)
Up-regulated (n = 22)	Down-regulated (n = 11)		
<i>Xdh</i>	<i>I11r11</i>	<i>ISG15</i> ^a	<i>ISG15</i> ^a
<i>Ly9</i>	<i>Hs3st1</i>	<i>LY6E</i> ^a	<i>LY6E</i> ^a
<i>Ccl2</i>	<i>Cdr2</i>	<i>LYZ</i> ^a	<i>LYZ</i> ^a
<i>Pla2g7</i>	<i>Galnt12</i>	<i>MS4A6A</i> ^a	<i>MS4A6A</i> ^a
<i>Mertk</i>	<i>Abhd6</i>	<i>IFITM3</i> ^a	<i>IFITM3</i> ^a
<i>Cdc42ep2</i>	<i>Klhl13</i>		<i>IFITM2</i>
<i>Nupr1</i>	<i>Plxdc2</i>		<i>VIM</i>
<i>Cd274</i>	<i>Siglech</i>		
<i>Tmem26</i>	<i>Fndc4</i>		
<i>P2ry14</i>	<i>Hpgd</i>		
<i>Nr1h3</i>			
<i>Ifit1</i>			
<i>Fam26f</i>			
<i>Gpr84</i>			
<i>Apoc2</i>			
<i>Cd84</i>			
<i>Slamf6</i>			
<i>Ctsd</i>			

^aOverlapping genes.